Summer 7-16-2021

Integrated Water Quality Monitoring of Skaneateles Lake Tributaries

Mengyi Zhang
Syracuse University

Abstract

Skaneateles Lake is the drinking water source for the City of Syracuse and surrounding areas. Harmful algal blooms (HABs) have been occurring in Skaneateles Lake every year since 2017 and posing a great threat to water quality and drinking water safety. Although the exact cause of the HABs is still unclear, sunlight, quiescent conditions, warm temperature, and elevated concentrations of nitrogen and phosphorus seem to favor the development of such blooms. In this study, a custom-built, low-cost, multi-parameter sensor unit was designed, built, and deployed on a third-order tributary. The unit collected high-frequency data for stage, temperature, pH, and dissolved oxygen. The unit successfully captured the variability in stream discharge calculated from stage measurements and temperature. The pH and dissolved oxygen sensors performed well during low-flow periods but deviated during high-flow events. Overheating of electronics also contributed to instability in sensor measurements.

Grab water samples were collected from nine tributaries and analyzed for total and dissolved organic carbon, phosphorus species, and nitrogen species. Nutrient analysis suggested export of phosphorus and nitrogen during high flow events. Analysis of physical watershed characteristics such as stream order, watershed area, and basin slope, implied that hydrologic flow paths were controlling the concentrations of some carbon, nitrogen, and phosphorus species.

This study could provide a blueprint for building low-cost water monitoring systems in non-navigational rivers and contribute to the understanding of how hydrological and nutrient dynamics influences HABs in lakes.

INTEGRATED WATER QUALITY MONITORING OF SKANEATELES LAKE TRIBUTARIES

by

MENGYI ZHANG

B.S., Qingdao Technological University, 2017

Thesis

Submitted in partial fulfillment of the requirements for the degree of

Master of Science in *Environmental Engineering*

Syracuse University

July 2021

Acknowledgment

To start with, I would like to show my gratitude to Dr. Svetoslava Todorova, who has been an excellent academic advisor and friend. Her attitude seeking for truth and extraordinary patience supported me through the difficulties during my adventure.

I also want to thank my defense committee for joining my defense online during this special time. Each of them has dedicated their time and provided valuable suggestions for my thesis.

I would never get the chance of studying abroad without the supports from my mom and dad. Rather than constraining me by their tender love and care, they encouraged me to see the colorful world with my own eyes and embrace other cultures with an open mind.

It is such a good fortune to have so many friends sharing good time and support each other's back when needed. Zhaowei Jiang, Yinding Chi, always visit me when I feel stuck in research; Priyanka Rajashekar and her husband provided huge help all the time, especially during our moving period; Hayley Van Duyn and her families are always on the phone for me. Without them, I would never survive the darkest hours. A special thanks to my boyfriend, Yueming Song, and my British short hair cat, Mimi. They have suffered from the noise of my Ukulele, my singing, and my boxing, but still gave me constant love and support the whole time: twenty-four hours a day, seven days a week.

Last but not least, I have to present my appreciation to Mike and Mario. Without their generous help in laboratory, it would take much longer time for me to get all the chemical analysis results.

Table of Contents

CHAPTER 1 Introduction

The rapidly growing human activity over the last decades is having a devastating impact on our planet. Overpopulation, pollution, consumption of fossil fuels, and deforestation have triggered negative effects including climate change, soil erosion, poor air quality, and undrinkable water. One of the recurring environmental events, harmful algal blooms (HABs), are closely associated with anthropogenic influence. HABs have attracted great public attention since last century because of their direct aesthetical damage on aquatic environments and effects to tourism and fishing industry. This study is aimed to better understand the nature of eutrophication in lotic (flowing water) systems utilizing high-frequency sampling by a custom-built multi-parameter sensor unit and grab sampling for chemical analysis.

Cyanobacteria and Eutrophication

Cyanobacteria, commonly referred to as blue-green algae, is a family of aquatic photosynthetic microorganism that were one of the earliest organisms on Earth. They act as producers in the ecosystem, providing food for fish and other consumers, also supplying oxygen during the photosynthesis process. But blue-green algae can be harmful to the environment when associated with eutrophication.

Eutrophication is a state of an ecosystem with increasing nutrient concentrations and aquatic organism activity (Thienemann, 1918). Eutrophication can be naturally enhanced by autochthonous production and recirculation (Wetzel, 2001). However, human activities can easily dominate natural processes and greatly increase the nutrients concentrations in aquatic

environments (Moss et al., 2013). Nowadays the term generally indicates phytoplankton enrichment caused by anthropogenic nutrient inputs. Human-controlled inputs can be traced back to the application of nitrogen (N) and phosphorus (P) fertilizers, growing of leguminous crops that fix N, and combustion of fossil fuels that discharges oxidized N into the air (Rabalais, 2002).

Though eutrophication and HABs are among the most important consequences of nutrient runoff, some N and P compounds may have more direct harmful effects on the ecosystem. High concentrations of ammonia (NH_4^+) dissolved in water are toxic to aquatic animals, especially at a higher pH level (EPA, 2013a). Nitrate (NO_3^-) has been reported to cause methemoglobinemia in infants at levels higher than 10mg/L (Fewtrell, 2004). There is also evidence indicating NO_3^- to be an endocrine disruptor for human bodies (Poulsen et al, 2018). During the 20th century, population and agriculture were both growing fast in North America, and environmental problems associated with eutrophication were gradually surfacing and drawing public attention. In the 1960s, Dr. Thomas Edmondson suspected that Lake Washington was experiencing cyanobacterial blooms because of the sewage discharge from the city of Seattle. In response to his public warnings, wastewater from Seattle was diverted from the lake into the nearby Puget Sound. Subsequently, algal blooms in the lake ceased and water quality improved remarkably in the lake (Edmondson, 1991). However, this solution for Lake Washington caused massive harmful algal blooms and shellfish poisoning in Puget Sound later on (Anderson et al., 2008). This phenomenon is frequently observed when nutrients are transferred from freshwater to marine continuum through linked water bodies (Paerl et al., 2018).

Lake Erie, one of the five Great Lakes in North America, went through similar issues. In the 20th century, over 12 million residents were depending on Erie's watershed, and sewage water from the cities was discharged into nearby shallow lakes. Algae blooms occurred, followed by depletion of dissolved oxygen (DO) caused by the decomposing algae in deeper part of the water, and a subsequent massive fish kill. Efforts were made to control P inputs to the Lake Erie, involving the restriction of phosphates in detergents and advanced wastewater treatment. As a result, the extent of algal blooms decreased and fish stocks were mostly recovered by the 1990s (Schindler et al., 2008). Unfortunately, there has been a recurrence of toxic cyanobacterial blooms in the Lake Erie since 2010, bringing endless trouble to local residents (Ho & Michalak, 2015).

Besides HABs, eutrophication can also disturb the ecosystem structure in lakes, rivers, and coastal environments. Increased N input can shift the dominating production species from benthic microalgal and macrophyte to pelagic species like phytoplankton, with dire effects for the entire submerged plant community (Moss et al., 2013). Since benthic invertebrates are the main food resource for fish, these changes reduce fish production (Vander Zanden & Vadeboncoeur, 2002). Furthermore, the algae will eventually die and consume oxygen when they decay, which exacerbates the habitat for other aquatic organisms.

In recent studies, more consequences of lake eutrophication have been revealed. Azevedo et al. (2013) observed that excessive P inputs reduce the biodiversity of the whole food web, with more impacts on streams than lakes. Beaulieu et al. (2019) predicted that enhanced eutrophication of lentic water systems (lakes and impoundments) would considerably increase methane emission from these water bodies (30-90%) over the next century, bringing

greenhouse effect equivalent to 18-33% of CO_2 emission from burning fossil fuels.

Research have shown that eutrophication is a direct result of increased nutrient loading. It was found that the correlation between phytoplankton growth and nutrients loading is stronger in lotic systems than lentic systems (Nieuwenhuyse and Jones,1996). An empirical analysis of global stream data found that summer mean chlorophyll concentrations, a proxy for algal biomass, increased from 20 to 180 mg m^{-2} when total N inputs increased from 500 to 3,000 μg L^{-1} and P inputs increased from 50 to 1,000 μg L^{-1} (Dodds & Smith, 2016). The relationship was stronger when N and P concentrations were considered together than either alone.

The N:P ratio entering a water body is a useful tool for assessing which nutrient may be the limiting factor for algal growth (Redfield, 1958). Studies found that P is likely to be the limiting nutrient when the ratio of N:P exceeds 14:1 (by mass). When N:P < 14:1, then P is likely to be abundant, and N is limiting algal growth. However, this metric is far from precise because various forms of nutrients have different bioavailability and each type of algae favors a certain combination of nutrients (Tank & Dodds, 2003). Maranger et al. (2018) proposed that a molar ratio of 25:1 (mass ratios of 11:1) should be used for freshwater ecosystems. Evaluating which nutrient limits algal growth helps researchers develop control and prevention strategies to better handle eutrophication.

Harmful Algal Blooms

Excessive nutrients input often leads to massive proliferation of phytoplankton, and when a particular toxic or harmful species dominates, cyanobacteria being the most common case in

freshwater systems, HABs occur. Blooms can develop from very few organisms when an ideal combination of certain physical, chemical, and biological conditions triggers its growth (WHO 2003). Blooms originate from resting cysts in the sediments. Some blooms proliferate at their origin, while others could originate in one location and be carried via wind-driven advection or upwelling events to another location. Generally, conditions favorable for developing algal blooms are abundant sunlight, quiescent conditions (especially after a storm), and sufficient nitrogen and phosphorus concentrations (WHO 2003).

HABs are believed to be one of the most disastrous events of human-related eutrophication (Paerl & Otten, 2013). The uncontrollable algal growth has multiple potential negative effects, including overgrowth and shading of seaweed and seagrass, oxygen depletion caused by phytoplankton respiration or decomposition of dead algal biomass, direct poisoning of fish and shellfish, suffocation of fish from stimulated gill mucus propagation, and mechanical interference with filter feeding plaguing fish and bivalve mollusks (Glibert & Burford, 2017). The economic damage of HABs and eutrophication in the U.S. is estimated to be a staggering $2.2 billion annually, largely attributed to losses associated with lake front properties and recreational use (Dodds et al., 2009).

HAB toxins can render freshwater resources unsafe for drinking, also unsuitable for irrigation and recreational purposes (Koreiviene et al., 2014). Some algal toxins are among the most potent toxins known to the world, even more poisonous per unit mass than cobra venom (Cheung et al., 2013). Liver toxins (hepatotoxins) are found in multiple cyanobacterial species, including the infamous wide-spread taxa, *Microcystis* spp., which dominated the third largest freshwater lake in China, Lake Taihu, in 2007. This bloom overwhelmed drinking water plants

in the Taihu Basin, leaving over 10 million local residents without drinking water supplies (Otten & Paerl, 2011). A study in 2015 also found significant association between algal bloom coverage and non-alcohol liver disease deaths in the U.S. (Zhang et al., 2015). In Brazil, 76 people in a clinic were killed in 1996 after drinking water containing high level microcystins, a notorious hepatotoxin produced by cyanobacteria (Carmichael et al., 2001).

Algal toxins can advance through the food web from herbivorous species to larger predators, with bioaccumulation and biomagnification effects (Grattan et al., 2016). Although acute poisoning of humans by cyanotoxins is uncommon, livestock are more frequently killed after drinking bloom-infested water (Stewart et al., 2008). Catastrophic bird mortalities caused by cyanotoxins have also been recorded (Alonso-Andicoberry et al., 2002). For humans and other land animals, the consumption of fish with bioaccumulated algal toxins is often the main path way of exposure (Grattan et al., 2016).

The intensity, frequency, and spatial distribution of algal blooms in freshwater ecosystems have been increasing since the 1980s (Ho et al., 2019). Freshwater aquatic systems in New York State are not immune to the problem. Several lakes in Upstate New York, such as Cayuga Lake, Chautauqua Lake, Conesus Lake, Honeoye Lake, Lake Carmel, Owasco Lake, Putnam Lake, and Skaneateles Lake all have experienced HABs in the last decade. There were 540 blooms recorded between 2012 and 2017 in the above-mentioned lakes, 168 of which were confirmed toxic (NYSDEC, 2017). Statewide, from 2008-2014, there was an average of 31 hospital visits per year associated with HAB exposure. From June to September 2015 alone, 35 cases of HAB associated illness that met the CDC case definition were reported, including 32 human cases and three of dogs. To mitigate the spread of HABs, water monitoring programs are urgently

needed to collect physicochemical parameters from water bodies and utilize them to develop damage control or prevention approaches.

Water Quality Monitoring

The history of watershed management can be traced back to as far as 2880 B.C. Even though the engineering techniques and documentations were lost during the Dark Ages, the knowledge of water quality analysis and watershed preservation was again pursued by scientists in the mid-19th century due to poor water quality associated with industrialization (Neary et al., 2009). Since then, global concern regarding the declining water quality of rivers, lakes and groundwater has catalyzed a reformation of water governance towards sustainable development through an approach, generally referred to as integrated watershed management (IWM) (Behmel et al., 2016). One of the major challenges posed by IWM is the need to build a reliable water quality monitoring program to track the status of a given watershed, so that decision makers can utilize the information for water management (drinking water processing, recreational and industrial use, water resource preservation and remediation, etc.).Water quality monitoring (WQM) can be described as a long-term program for measuring and analyzing water parameters in order to define the status and trends of an aquatic environment. From the 1960s to 2000, water sampling and analysis relied heavily on manual techniques. A researcher needed to travel to a water source, collect water samples, and bring these samples back to a laboratory for analysis. At that time, the focus of WQM projects was on the general framework and the network design. The first part involved the development of the objectives, as well as

specific strategies and tools to be used in the project. The network design determined which water quality parameters were to be measured, where to take samples, and how often were samples collected (Sanders, 1983). Some researchers found it necessary to build fixed sampling stations in order to approach the water body easily and collect water samples consistently (Strobl & Robillard, 2008). There were other studies emphasizing the importance of efficiently utilizing the collected data. For instance, techniques were perfected for converting raw data into a format that facilitates further processing and decision making (Chapman, 1996; Strobl & Robillard, 2008). These traditional WQM systems often failed to capture the quick temporal and spatial change of water properties (Katsriku et al. 2015). Moreover, extensive manual labor often leads to errors. Operational errors can be introduced during the sample collection, including sample cross contamination or misidentification, also during laboratory water quality analysis, data recording and data analysis. In addition, errors can come from tools used for collecting and transporting samples, such as the choice of containers for sample collection and transportation, the contamination of reagents and other environmental substances, and storage conditions like light and temperature. Some errors are induced by the laboratory equipment malfunction and miscalibration. More errors may appear while processing and reporting data, including statistical errors, round-off errors, and omission of values (van Niekerk, 2004).

Beginning from the late 2000s, with the invention of new technologies, advanced techniques were introduced to help resolve some of the limitations of the manual WQM approaches. Optical sensors, traditionally used for detecting visible impurities, were designed to measure DO, pH, turbidity, water level, and residual chlorine by applying a variety of active indicators (Bhardwaj et al., 2015). Micro-Electro-Mechanical Systems (MEMS) based on

nanotechnology use microcircuits to detect changes of the surrounding environment. MEMS-based sensors are capable of sensing water level, pressure, flow, temperature, and also heavy metal ions (Wu et al., 2020). MEMS-based sensors can significantly reduce the cost of the monitoring system because of its large-scale production. Biosensors are known for their high selectivity and sensitivity. Biological indicators interact with very specific targets, and a transducer is necessary for generating a signal. The greatest advantage of biosensors is their ability to provide not only chemical data, but also the corresponding biological effects (i.e. toxicity, endocrine-disrupting effects), which is often more meaningful than chemical composition alone (Rodriguez-Mozaz et al., 2006). Some water quality parameters can even be acquired remotely via satellite imagery (Sawaya, 2003).

To enhance data collecting and processing, sophisticated computing and telemetry technologies, such as the Internet of Things technology, microcomputer technology, and wireless communication technologies like Wi-Fi and Bluetooth, are emerging as new trends in WQM projects. Furthermore, the idea that some obtained data can be processed on the Internet and visualized on a website were introduced to design monitoring systems (Hall et al., 2007). Nowadays, new WQM has gradually substituted traditional manual water sample collection approaches with advanced automatic monitoring systems that allow water samples to be consistently collected and analyzed.

The Arduino Platform

When designing a monitoring device, an Input/Output (I/O) board performs the crucial task of

integrating all the different sensors together and record their collected data in real time. Microcontroller I/O boards are physical computing platforms consisting of a simple microcontroller and a development environment for software programming. Several manufacturers, such as Parallax Inc., Picaxe, and Coridium Corporation, have provided a variety of similar products (D'Ausilio, 2012). However, assembling and programming these boards require extensive knowledge of electronics and programming language. Therefore, Arduino emerged as the most popular I/O platform among users with little computer engineering expertise. Due to its open-source philosophy, hundreds of pre-programmed projects can be found online to be used or modified for specific needs. There are several web tutorials guiding basic programming and device assembling, and active communities available for help.

A selection of circuit boards can be found to develop an Arduino platform. Most of these boards use Atmel's low-power CMOS 8-bit microcontrollers based on AVR enhanced RISC architecture. The performance of these microcontrollers allows them to compute approximately 300,000 lines of program code per second, which is capable enough for regular data input and output applications necessary for water quality data collection. The software part includes a standard programming language and a firmware that runs on the board. Arduino programming uses a simplified version of C/C++ language in an integrated development environment (IDE). Arduino boards are also highly compatible with other functional software such as Flash, Processing, MaxMSP, and MATLAB, and a few lines of code is often enough to complete very useful tasks.

The objective of this study is to develop an integrated water quality system for monitoring non-

navigational rivers. To achieve this, the study focused on two main goals: 1) to build an Arduino-based multi-parameter water quality monitoring system for high-frequency monitoring of general water parameters such as DO, pH, flow and temperature, and 2) to collect baseflow and high flow samples and determine the change in concentration of N, P, and carbon (C) species. This project took advantage of the Arduino-based architecture. The hardware part of the Arduino-controlled sensor unit is cost-effective. Combined with laboratory data, this system should be able to produce integrated information for tracing conditions leading to eutrophication and HABs. It could provide invaluable infrastructure for further water quality control and HAB management projects.

CHAPTER 2 Site Description

Skaneateles Lake is one of the Finger Lakes in central New York, United States, formed during the most recent glaciation period (Pleistocene). The lake is about 25 km long, 2.4 km wide (at its widest location), and has a surface area of 35.9 km^2 (Figure 2.1). At its deepest location, the lake is 90.5 meters deep. Skaneateles Lake is dimictic, with strong stratification during the summer; complete mixing occurs in the spring and fall. Skaneateles Lake is classified as oligotrophic due to its low nutrient loading (Abbot, 2019) and is a Class AA waterbody, i.e. best use for drinking water purposes, according to the New York State Department of Environmental Conservation (NYSDEC). Skaneateles Lake is the primary source of drinking water to the City of Syracuse, village and town of Skaneateles, and the adjacent villages. NYS Department of Health and the USEPA have issued a filtration avoidance waiver for Skaneateles Lake in 2004 due to the high quality of the water in the lake. The waiver allows water to be delivered to the customers without sophisticated treatment, only following a coarse sand filtration and chlorination. The waiver remains in effect indefinitely as long as the City of Syracuse maintains the quality of the water within the guidelines set by the waiver (NYSDEC, 2017).

The Skaneateles Lake watershed is 154 km^2 and consists of 52% shrub and pasture, 37% forest, 6% residential and commercial land, and 5% wetlands and open water (Figure 2.2). The watershed to lake surface area ratio is about 5.3, the lowest among the eleven Finger Lakes. The watershed to lake surface area ratio for the other Finger Lakes is between 9.8 and 18.7 (NYSDEC, 2017). Based on inflow-outflow and runoff data, the water residence time in the

lake is estimated to be between 14 to 18 years (Michel & Kraemer, 1995).

There are about 150 tributaries discharging into Skaneateles Lake. Not all the streams are perennial, having flow year-round. Some of the streams are intermittent and cease flowing during dry months; others are ephemeral and flow only after rain events. Due to the narrow shape of the watershed, most of the streams are first order or second order (Figure 2.1). Only the largest stream, Grout Brook, which flows into the southernmost part of the lake, has a USGS station for continuous monitoring of the flow.

This study focused on nine of the tributaries: Bentley Brook, Dowling Creek, Fisher Brook, Five Mile Creek, Glen Cove, Hardscrabble Brook, Mile Point Creek, Ten Mile Creek, and Willow Brook.

Bentley Brook (42.907, -76.419, #3 on Figure 2.1) is a second order stream located on the west side of Skaneateles Lake, approximately 5.8 km from the Village of Skaneateles. The creek, which is the largest of the tributaries in this project, has a drainage area of 4.03 km^2. About 61% of the drainage area is comprised of agricultural land (2.46 km^2), 13% is wetland (0.54 km^2), and 10% is developed area (0.42 km^2). The rest of the drainage area is mostly forested (0.37 km^2). Bentley Brook has both the largest agricultural land, developed land, and wetland areas of the nine creeks studied.

Dowling Creek (42.928, -76.429, #2 on the Figure 2.1) is a second order stream which is located close to the Village of Skaneateles. This creek has a drainage area of 1.29 km^2 and with mostly agricultural land (72%) with an area of 0.93 km^2. The rest of the watershed is developed land (25%) with an area of 0.33 km^2.

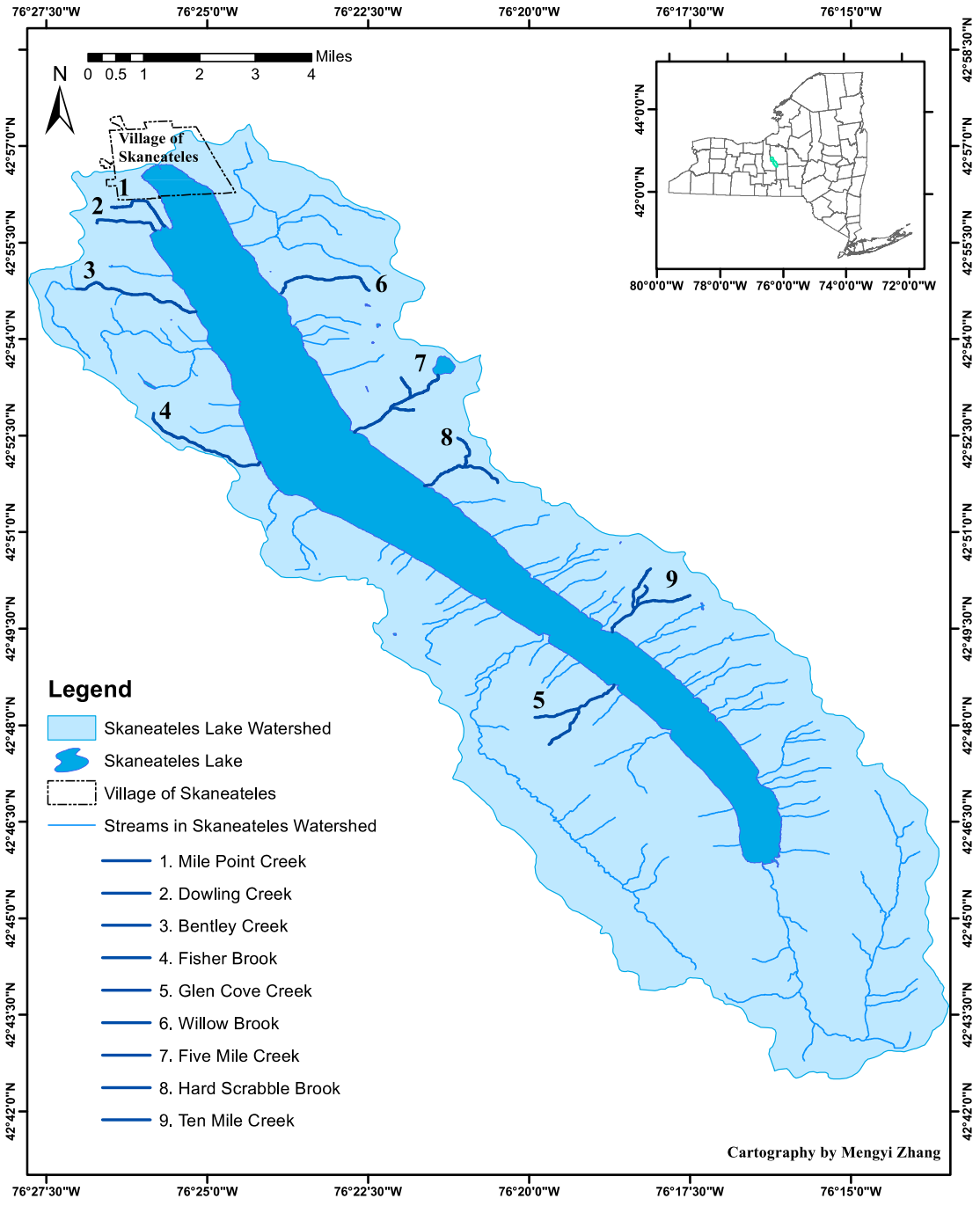

Figure 2.1: Map of Skaneateles Lake watershed, with locations of study sites.

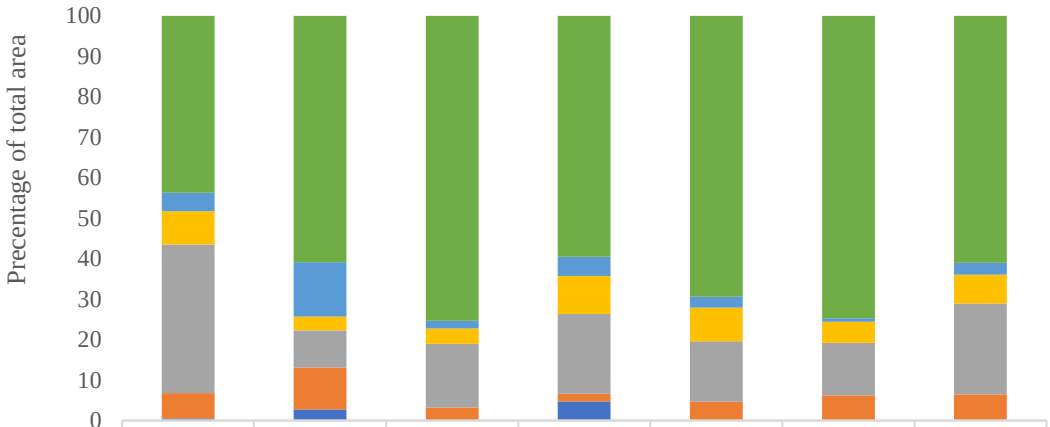

	Skaneateles Lake	Bentley Creek	Fisher Brook	Five Mile Creek	Glen Cove Creek	Hard Scrabble Brook	Ten Mile Creek
Agricultural Land	43.74	60.87	75.32	59.50	69.44	74.74	61.02
Wetlands	4.57	13.45	1.92	4.81	2.65	0.81	2.90
Shrub/Grassland	8.22	3.41	3.77	9.35	8.29	5.24	7.19
Forest	36.73	9.17	15.79	19.74	15.00	13.00	22.45
Developed	6.21	10.33	3.20	1.87	4.62	6.21	6.44
Open Water	0.52	2.77	0.00	4.73	0.00	0.00	0.00

Figure 2.2: Land cover characteristics of Skaneateles Lake and its tributaries.

Fisher Brook (42.868, -76.403, #4 on Figure 2.1) is a first order stream located on the western side of Skaneateles Lake. It is approximately 10 km south from the Village of Skaneateles. The drainage area of the creek is 1.41 km^2. Land cover is primarily agricultural (75%) with an area of 1.06 km^2. The rest of the drainage area is mostly forested (16%) with an area of 0.22 km^2.

Five Mile Creek (42.876, -76.378, #7 on Figure 2.1) is located on the eastern side of the lake. It has a drainage area of 3.37 km^2. The watershed is primarily agricultural (60%) with an area of 2 km^2 and forested area (20%). Five Mile Creek has the largest open water/wetland (0.16 km^2), shrub/grassland (0.32 km^2), and forested (0.67 km^2) areas of the study streams (Figure 2.2).

Glen Cove (42.810, -76.311, #5 on Figure 2.1) is on the western side of the lake with a basin of 2.28 km^2. The drainage area is dominated by agricultural land (70%) with an area of 1.58

km^2. The rest of the drainage area is mostly forested (15%) with an area of 0.34 km^2.

Hardscrabble Brook (42.862, -76.360, #8 on Figure 2.1), is located on the eastern side of Skaneateles Lake, south of the Five Mile Creek. It has a drainage area of 2.33 km^2. The land cover is dominated by agricultural land (75%) with an area of 1.74 km^2; the rest of the watershed is covered by forest (13%) of 0.3 km^2.

Mile Point Creek (42.929, -76.427, #1 on the Figure 2.1) is a second order stream near the village of Skaneateles. About 55% of the watershed is agricultural land (0.57 km^2) and 40% is developed land (0.42 km^2). The remainder of the drainage area is forested (0.056 km^2).

Ten Mile Creek (42.824, -76.312, #9 on Figure 2.1) is located on the eastern side of the lake with a basin of 2.42 km^2. The stream is intermittent and dries out during the dry summers. The land cover is mainly agricultural land (61%) with an area of 1.48 km^2 area, and the rest of the watershed is mainly forest (22%) with an area of 0.54 km^2.

Willow Brook (42.911, -76.398, #6 on the Figure 2.1) is a third order stream located on the eastern side of the lake. It has a drainage area of 2.10 km^2. The land cover is dominated by agricultural land (55%) with an area of 1.15 km^2; and the rest of the watershed is covered mainly by forest (41%) with an area of 0.86 km^2. The developed land (4%) of the drainage area is 0.09 km^2.

CHAPTER 3 Methods

Arduino System

System Block Diagram

Arduino an open-source hardware and software platform. The platform consists of three subsystems: data acquisition, data processing, and data storage (Figure 3.1). The introduction of three subsystems follows the direction of data flow. Data collection subsystem consists of sensors detecting water quality parameters. Arduino Leonardo A000057 microcontroller was used for data processing. The current data saving subsystem utilized a secure digital (SD) card.

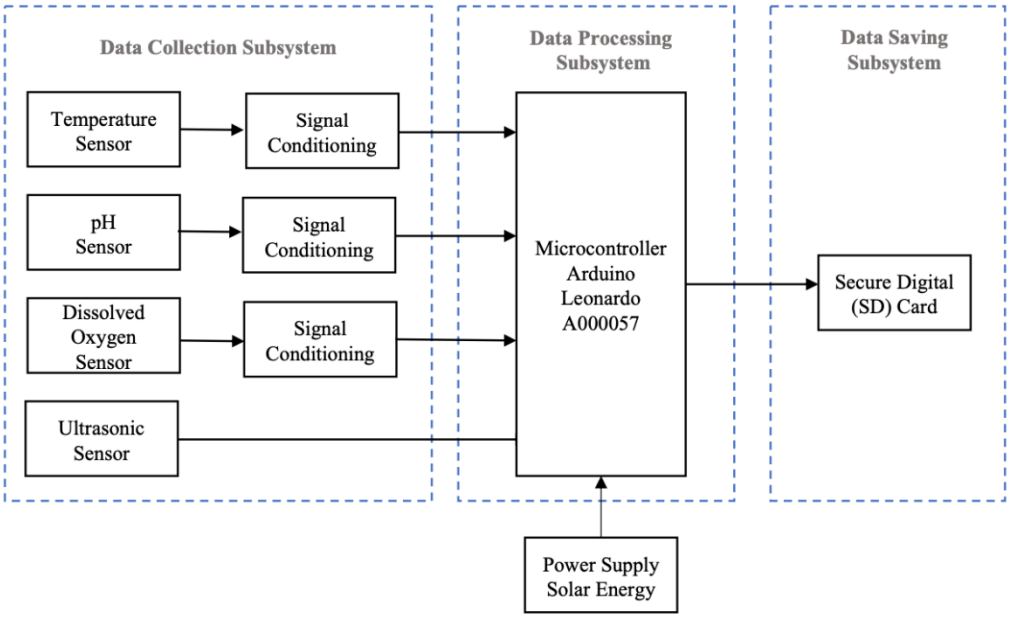

Figure 3.1: Water quality monitoring system block diagram

Data collection subsystem is the forefront of the system, which directly connects with external environment, in this case, the stream water. Four water quality sensors were connected to detect temperature, pH, DO, and an ultrasonic sensor for depth measurement. The detection range, accuracy of the sensors, and manufacturer are given in Table 3.1.

Table 3.1 Specifications of sensors

Sensor	Detection range	Accuracy	Manufacture
Temperature	-126℃~1254℃	±0.1℃	Atlas Scientific
pH	0.001~14.000	±0.002	Atlas Scientific
Dissolved Oxygen (DO)	0.01mg/L~100mg/L	±0.05mg/L	Atlas Scientific
Ultrasonic Sensor	2cm~800cm	±1%	DFRobot

The ultrasonic sensor (DFRobot, Shanghai, China) was used to estimate the stage (water level) in the creek by measuring the distance between the sensor (mounted at the bottom of sensor box) and the stream surface. To calculate the stage, the distance measured by the sensor was subtracted from the total distance from sensor to the bottom of the stream bed. The speed of sound was corrected for temperature.

The data processing subsystem functions as the minicomputer, converting electric signal to digital format, and translating it to measurements by designed equations. All these functions were performed by a microcontroller, Arduino Leonardo A000057 development board (Figure 3.2). The Arduino Leonardo is an ATmega32u4 microcontroller that contains 18 general purpose input/output (GPIO) pins to connect with the external hardware devices, in this case the sensors.

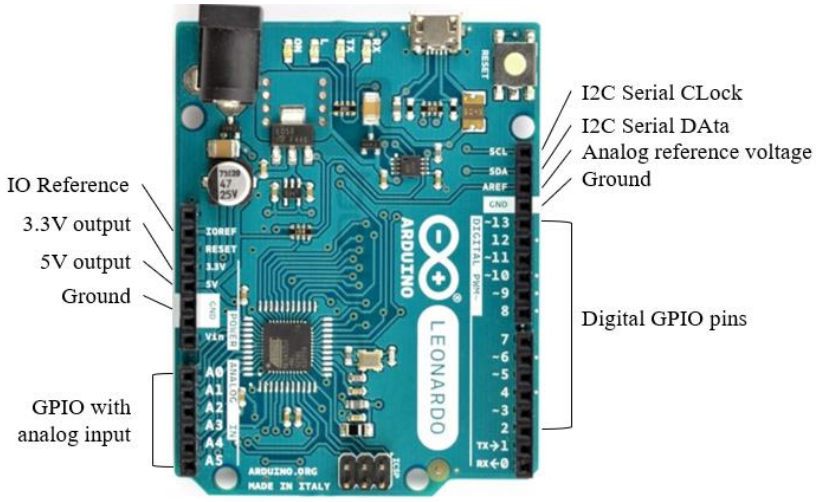

Figure 3.2: Arduino Leonardo A000057.

The data saving subsystem consisted of a USB port and a SD card. USB port allowed connection with a laptop. The data were saved in SD card and retrieved weekly.

System Design

The Arduino hardware system had four sensors attached to the Arduino Leonardo board by breadboard (Figure 3.3). The system was powered by a solar panel (DFRobot, Shanghai, China) with back up lithium-ion battery (Adafruit, New York, NY).

The temperature, pH, and DO sensors were attached to I^2C Serial Clock (SCL) and I^2C serial Data (SDA) pin for data transmission. Voltage isolators were added (EZO Inline Voltage Isolator v6.0) for pH and DO circuits to reduce the electrical noise (micro-voltage coming from other sources and other sensors on the same board), Atlas Scientific Basic EZO Inline Voltage Isolator v6.0 was used. Two isolators were individually attached to the VCC pin on pH and DO circuits. Then temperature, pH isolator, and DO isolator were attached to SCL and SDA. Ultrasonic sensor was attached to pins 8 and 9 of the Arduino Leonardo (Figure 3.3).

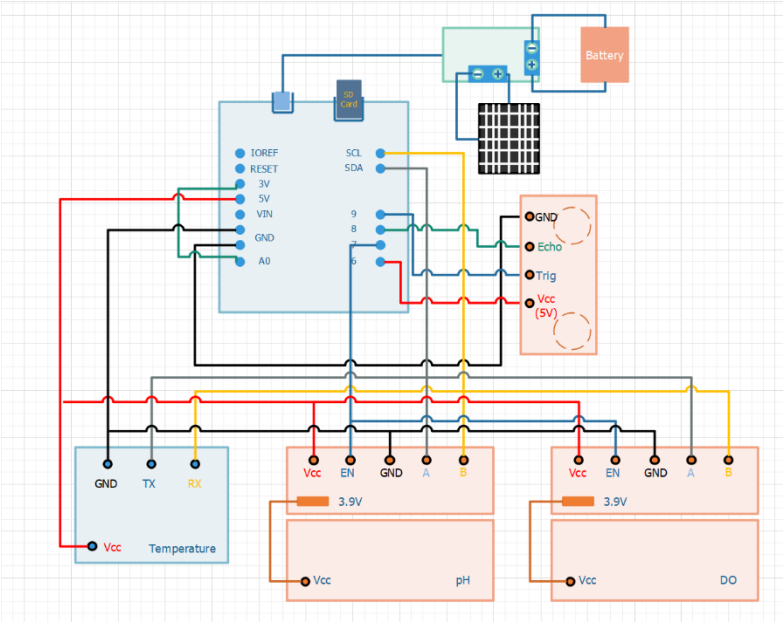

Figure 3.3: System circuit diagram.

The custom-built multi-parameter sensor unit was housed in a water-proofed hinged box (Polycase ECP Coer., Chester, OH) and attached on a bridge over the creek by two clamps (Figure 3.4). The components of the custom-built multi-parameter unit are listed in Table 3.2.

Figure 3.4. Field installation of the custom-built multi-parameter Arduino sensor unit.

Table 3.2 Individual and total component costs for the Arduino unit in this project

Component	Model	Manufacturer	Supplier	Cost ($)
Waterproof Box		Polycase Corp.	Polycase.com	44.71
Microcontroller	Arduino Leonardo A000057	Arduino	Digikey.com	19.8
Temperature Probe & Circuit	PT-1000 Temperature Kit (#KIT-301)	Atlas Scientific	Atlas-scientific.com	68
pH Probe	ENV-45-pH Probe	Atlas Scientific	Atlas-scientific.com	60.5
pH Circuit	EZO-pH Circuit	Atlas Scientific	Atlas-scientific.com	40
Voltage Isolator for pH	Basic EZO Inline Voltage Isolator (#BE-IVI)	Atlas Scientific	Atlas-scientific.com	26
DO Probe	ENV-40-DO Probe	Atlas Scientific	Atlas-scientific.com	218
DO Circuit	EZO-DO Circuit	Atlas Scientific	Atlas-scientific.com	46
Voltage Isolator for pH	Basic EZO Inline Voltage Isolator (#BE-IVI)	Atlas Scientific	Atlas-scientific.com	26
Ultrasonic Sensor	URM37 V5.0 Ultrasonic Sensor	DFROBOT	dfrobot.com	13.9
			TOTAL COST	562.91

Software Design

The program for custom-built multi-parameter Arduino unit was written with Arduino integrated development environment (IDE) software based on the C++ language. The IDE is supplied by Arduino Codes. A real-time clock module was added to the system, a code was downloaded from Adafruit.com, and added on the Arduino Library. The real-time clock keeps track of the current time. It was programmed to turn on only during data collection. The unit was operated with detection intervals of three to five minutes. Quiescent state was implemented for power saving.

Functional Testing of Depth Measurements

The performance of the custom-built multi-parameter sensor unit on depth measurement and temperature were evaluated using HOBO U20 Water Level Logger. The HOBO logger contains sensors that measure simultaneously pressure and temperature. A pair of HOBO pressure transducers were installed at Five Mile Creek in August and September 2019. One of the pressure transducers was attached to the bridge by cable tie to measure atmospheric pressure,

and the other one was submerged at the bottom of the creek, fixed to the PVC pipe, which housed the sensors.

The depth of the stream was calculated using the pressure difference between the bottom of the creek and atmospheric pressure ($P_{under\ the\ water} - P_{above\ the\ water} = \rho g h$, where h is the stage of the creek). The temperature obtained from the pressure transducer submerged in the creek was also compared with the temperature data obtained from the custom-built multi-parameter sensor unit.

Rating Curves and Estimates of Streamflow

Stream gauging was initiated for five of the streams- Bentley Brook, Fisher Brook, Five Mile Creek, Hardscrabble Brook, and Willow Brook, but more precise gauging was done for Five Mile Creek. Flow was calculated by a statistical stage-discharge relationship (called rating curve) using discharge (represent by Q, [m^3/s]) on x-axis versus stream water depth (called stage, represent by H, [m]) on y-axis. To obtain discharge, the cross-section area of the stream (represent by A, [m^2]) and the velocity (represent by V, [m/s]) in the stream were measured. Note that a minimum of 64 cm (2.5 inches) of water depth is required for velocity meter to work properly. Therefore, some measurements were obtained by other methods. The graphic presented in Figure. 3.5 is a cross-sectional area of the stream channel of Five Mile creek. It depicts the method used to calculate the discharge.

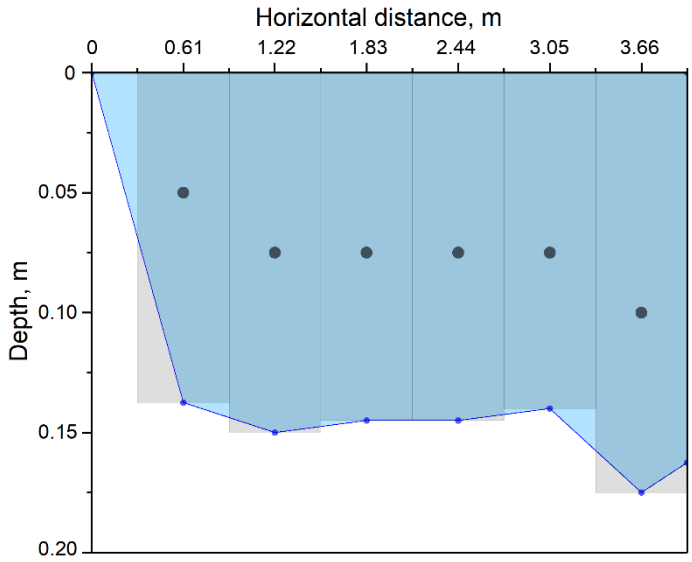

Figure 3.5: A cross-section of Five Mile Creek. Horizontal distance is the distance from one bank to another, which is around 4 m (13 ft). Gauge heights (stage) were measured every 0.61 m (2 feet). Dots represent the approximate location of velocity measurements.

To determine the cross-sectional area, the tributary was divided into two-feet sections (Figure 3.5). Two stakes were positioned on both sides of the stream and a string was tightened to the stakes to mark a line above the stream. Starting from one end, depth and velocity were measured every 0.61 meters (2 feet). A field ruler was used to measure the depth. For each of the cross-sections A_i, the area in m^2 was calculated using the formula:

$$H_i * 0.61 = A_i \tag{3.1}$$

where H_i represents the depth at each cross-section in inches, and A_i. A portable velocity meter was used to measure the steam flow velocity (Marsh-McBirney, Inc, Model 201). The discharge in m^3/s was calculated using the formula:

$$Q = \sum_{i=1}^{N} A_i * V_i \tag{3.2}$$

where A_i is the area of each cross-section in m^2, and V_i is the velocity in the center of the cross-

section in m/s. Once the rating curve was developed, the relationship was used to determine the discharge only by a single measurement of the stage in the creek.

Precipitation Data

The precipitation data were obtained from the Northeast Regional Climate Center RCC Climate website built by Cornell University (**http://climod2.nrcc.cornell.edu/**). The historical record was obtained for the station for Skaneateles Lake Village (42.946, -76.431). It should be noted that the NERCC database provides only cumulative daily precipitation.

Sample Collection and Analysis

Water samples for chemical analysis were collected biweekly from August 2018 until April 2019. Samples were collected weekly in May and June 2019 and then resumed the biweekly collection until February 2020. Joint efforts between our research team and citizen volunteers, trained by Syracuse University and the Skaneateles Lake Association, allowed additional collection during and after storm events. All data collected between August 2018 and February 2020 were used for analysis in this study.

Grab samples were collected from the middle part of each stream to avoid agitation. Standing water near stream banks was not collected because it was not well mixed and does not represent stream conditions. Before collecting the samples, the bottles were rinsed three times with stream water, then suspended into the water facing upstream and slowly filled to limit collection of bottom sediments and detritus. Bottles were labeled individually and stored in ice-coolers

maintaining 3-5 °C until transferring to the laboratory at Syracuse University.

All samples were collected in 250 mL clear glass Boston Round Bottles to prevent loss or exchange of matter through the bottle wall due to diffusion or evaporation. These bottles have narrow screw neck opening and round body, which can minimize chemical interference with air. Before being used in the field, the bottles were rigorously cleaned following the procedure outlined here. The bottles were rinsed six times with tap water, autoclaved, filled with 1N hydrochloric acid solution (HCl) for 24 hours, and rinsed six times with deionized water (DI water). The first rinse with DI water was disposed in a designated waste container for neutralization. Bottles were filled with DI water, capped, and sat for 24 hours. Lastly, the caps and bottles were rinsed again, inverted, and dried 24 hours.

Water samples from all nine tributaries were analyzed for organic carbon, phosphorus, and nitrogen species. Analyses were done for total organic carbon (TOC), dissolved organic carbon (DOC), total phosphorus (TP), soluble reactive phosphorus (SRP), total dissolved phosphorus (TDP), nitrate and nitrite (NO_x), and ammonia (NH_4^+). Proper quality assurance and quality protocols were followed to assure dependability and traceability of the data.

Organic Carbon Species

Samples for TOC and DOC were analyzed using Phoenix 8000 TOC Analyzer (Teledyne Tekmar). Samples for DOC were filtered through 0.45 μm polyester (PES) filters (EZFlow Syringe Filter, diameter of 25 mm) using 60 mL syringe and a filter cassette. The filtrate was collected in 40 mL glass vials and stored under 3-5°C prior to analysis. The glass vials were rinsed six times with DI prior to filtration. The filter was rinsed once by pushing three 10 mL of DI water through the syringe. After the initial rinse, the filter was removed, followed by the

syringe plunger, and then 50 mL of sample was poured into the syringe. This sequence was important to assure that that the filter will not be compromised by the pressure. The first 15 mL pushed through the filter were discarded, and the rest of the filtrate was collected in the glass vial. Each sample was filtered through a different filter.

Filtered water samples were analyzed for DOC following USEPA Method 415.3 (Potter and Wimsatt, 2009). The organic carbon in the water was oxidized with a combination of heat catalyzed chemical oxidation with sodium persulfate ($Na_2S_2O_8$), phosphoric acid, and UV irradiation to produce carbon dioxide (CO_2). The results are reported as mass of carbon per volume of sample. Non-filtered samples were analyzed with the same analytical procedure to determine TOC.

The precision of the analysis was evaluated using initial and continuous laboratory control samples such as Initial Calibration Verification (ICV) prior to any samples in analysis, Initial Calibration Blank (ICB) following the ICV, Continuing Calibration Verification (CCV) after every ten samples, and Continuing Calibration Blank (CCB) following each CCV. The recovery of the laboratory control samples was calculated using the formula:

$$\text{Recovery (\%)} = \frac{\text{Measured Concentration}}{\text{Stanadard Concentration}} \times 100 \quad (3.3)$$

All recoveries were between the recommended range of 90% and 110%, with the average of 100.91±5.20% (average±standard deviation).

Nitrogen and Phosphorus Species

The non-filtered water samples were analyzed for NH_4^+, NO_3^-, SRP, and TDP using the segmented flow analyzer system, SEAL AA500 Autoanalyzer (Seal Analytical Inc.). Each sample was simultaneously analyzed for the four chemicals of interest. SRP was measured by

forming a yellow-colored antimony-phospho-molybdate complex, which was reduced by ascorbic acid to a blue-colored antimony-phospho-molybdenum complex. A photometer detects the intensity of the blue color at 660 nm wavelength (red-light). SRP concentration is proportional to intensity of the color.

TDP was measured by digesting the sample with persulfate to release the organic bound phosphorus and convert it to SRP, which was then measured with the method described above. To determine NO_3^- concentration, NO_3^- was reduced to nitrite (NO_2^-) using granulated copper-cadmium at pH of 8.5. Then NO_2^- reacted with sulfanilamide under acidic conditions to form a reddish-purple colored complex (azo dye). The intensity of the colored solution was measured colorimetrically at 520 nm. NH_4^+ was detected by chemically forming indophenol blue. The intensity of the color was measured cholorimetrically at 630 nm.

Instrument precision was verified by methods blanks and ongoing precision and recovery samples, such as ICV, ICB, CCV, and CCB. Recoveries of the ICVs and CCVs were calculated using Eq. 3.1 and were between 90% and 110%. For nitrate (NO_3^-), the average recovery was 103.06±4.50%; for ammonia (NH_4^+), average was 101.62±2.88%; for OP, average was 102.52±3.74%; and for TDP, the average was 103.06±2.46%.

Total Phosphorus

TP was determined using inductively coupled plasma, mass spectrometry (NexION 2000 ICP MS, Perkin Elmer). Samples we acidified with 1% nitric acid and 1% hydrochloride prior to analysis for the phosphorus in compound to be dissolved. To determine the concentration of TP, samples were dissociated into atoms and directed into mass spectrometer which separates the elements by various mass-to-charge ratio. The ions went through detector and were

amplified into measurable pulse. The concentration of the elements is obtained by comparing the intensities of the pulses with standards.

The precision of the measurement was evaluated by the recovery of the CCVs. Recoveries of the CCVs were calculated using Eq. 3.1 and were 101±5.12%. Duplicates samples were run with every batch and the Relative percent difference (RPD) between the duplicates was calculated. The RPD of the laboratory control samples was calculated using the formula:

$$\text{RPD} = \frac{|X_1 - X_2|}{(\frac{X_1 + X_2}{2})} \times 100 \quad (3.4)$$

where: X_1 and X_2 are measurements of the duplicate sample. All RPD for TP were 6.43±3.27%.

Commutative and Statistical Analysis

Carbon species were categorized into TOC, DOC, and suspended organic carbon (SOC), the latter one calculated as the difference between TOC and DOC.

Nitrogen species considered for the analyses were total nitrogen (TN), organic nitrogen (ON), and dissolved inorganic nitrogen (DIN). DIN represents nitrogen oxides (NO_3^- and NO_2^- or NO_x), and ammonia (NH_4^+). While NO_x and NH_4^+ were directly measured in the laboratory, ON was derived by subtracting DIN from the TN concentration.

Phosphorus species included in the analyses were TP, suspended phosphorus (SP), TDP, SRP, and dissolved non-reactive phosphorus (SnRP). Suspended P concentration was calculated by subtracting TDP from TP. SnRP was determined as the difference between TDP and SRP.

Statistical analyses were carried out with SPSS Statistics for Windows, Version 27.0 (IBM Corp., 2021). A one-way analysis of variance (ANOVA) was applied to evaluate the differences in nutrient concentrations between creeks and seasons. Post-hoc analysis on simultaneous

pairwise comparison was done using Tukey's test. All significant differences were evaluated using 95% confidence ($p < 0.5$).

CHAPTER 4 Measuring Physical Parameters and Flow with a Custom-built Multi-parameter Unit

Introduction

The electronic revolution has opened new opportunities in water monitoring. The advances in sensor technologies, mobile computing, and wireless communications now allow scientists to acquire, process, and transmit an array of data in the field, or remotely from off-site laboratories. Robust *in-situ* monitoring of major physical and chemical parameters (temperature, pH, conductivity, turbidity, DO, and chlorophyll) has been achieved with deployable platforms (buoys), capable of rapid profiling and remote data acquisition in lakes and large rivers. Stream flow has been estimated by continuous measurements of water levels and completion of time-series from gauge-specific rating curves. However, these monitoring systems have been utilized mainly in larger aquatic systems.

Establishment of an operating station for continuous flow and water quality measurement could become expensive and unjustified for non-navigational, small, and intermittent creeks. Therefore, these rivers are monitored irregularly and by the traditional manual approach with commercial hand-held water quality probes and periodic measurements of flow. The cost efficiency, time, and travel for personnel are the major obstacles for building extensive and continuous water monitoring networks. For instance, despite that the US Geological Survey (USGS) maintains a stream gauging network on 10,330 streams, there are only 13 stations in the Finger Lakes region, a home of 11 lakes, all of which have experienced algal blooms of different severity in the last decade. The glacially created Finger Lakes have narrow watersheds

with sometimes hundreds of short-length, low-order streams. These streams are not good candidates for deployment of continuous multi-sensor platforms. For them, low-cost sensor units have the potential to provide an affordable solution.

The wide availability of microcontrollers, such as Raspberry Pi and Arduino, have spurred the utilization of low-cost modules and sensors for water quality measurements. Different research groups have started developing sensor modules that measure one parameter (Mulyana & Hakim, 2018; Trevathan et al., 2020; Y. Wang et al., 2018). There are only a few published studies that report the development of an Arduino-based multi-sensor unit for continuous monitoring (Assendelft & Ilja van Meerveld, 2019; Osman et al., 2018). In some of these studies, the verification of the customized multi-sensor units has been done only under laboratory conditions (Osman et al., 2018). To my knowledge, only one study has reported the successful operation of a customized multi-sensor unit in the field (Assendelft & Ilja van Meerveld, 2019). The unit was installed at multiple locations in a small headwater watershed for nine months and measured temperature and flow.

In my study, I document the development and field verification of an Arduino-based low-cost sensor unit for continuous monitoring of temperature, DO, pH, and water depth at a perennial, second order stream in Skaneateles Lake, NY watershed. The Arduino open-source platform, which includes both software and hardware, enabled the development of the unit that is less than 8% of the cost of the commercially available multi-parameter models.

Results

Functionality Testing

To test the functionality and accuracy of the ultrasonic sensor, the stage and temperature data obtained by the custom-built multi-parameter unit were compared to those obtained by a pair of HOBO pressure transducers. The test was conducted from August 23rd to September 5th, 2019, and from September 25th to September 29th, 2019 at Five Mile Creek.

The comparison between the ultrasonic sensor and the pressure transducer showed that the data from the sensor unit is slightly lagging compared to the data from the pressure transducer. The real time clock in the sensor box appears to be making readings at intervals slightly over 3 minutes - 3 minutes and 3 seconds or 3 minutes and 4 seconds. However, the pressure transducer reads data at 3 minute-intervals (Figure 4.1).

The water level in the Five Mile Creek depicted by the ultrasonic sensor and the HOBO pressure transducers showed similar patterns. Both sensors captured well the high flow events on August 28th, September 2nd, and September 29th (Figure 4.1 B and 4.1 D). The water depth measured by the ultrasonic sensor was always higher than the estimate obtained by the pressure transducers. During the first testing period (August 23rd - September 5th), the ultrasonic sensor reported water depth at baseflow of 12±0.67 cm (average ± standard deviation), while the HOBO pressure transducer reported water depth of 8.4±0.3 cm. At the time of deployment (August 23rd), the stage in the creek was measured to be 14.2 cm. The value obtained by the custom-built multi-parameter unit on August 23rd was 14.1 cm. Similarly, during the second testing period (September 25th - 29th), the ultrasonic sensor measured water level at baseflow of 9.7±0.4 cm and the pressure transducer reported water depth of 7.6±0.4 cm. The stage at the

time of deployment (September 25th) was measured to be 10.4 cm, comparable to the stage obtained by the custom-built multi-parameter unit of 9.9 cm on that day. The discrepancy in the water level readings between the pressure transducer and the ultrasonic sensor increased during high-flow events (Figure 4.1 B and 4.1 D). It should be noted that the pressure transducer in the creek was deployed so that it just touched the soft bottom of the creek but did not sit firmly on the bottom. This position was chosen to prevent sediment buildup on the unit and avoid potential malfunction of the pressure sensor.

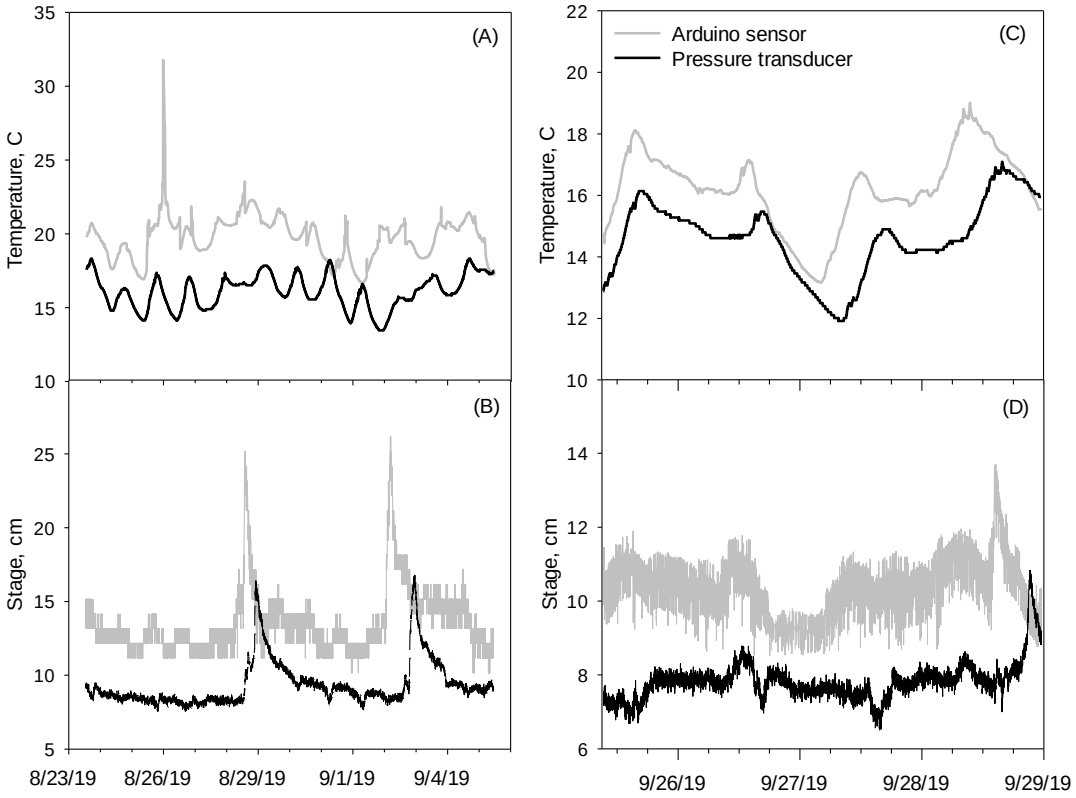

Figure 4.1: Comparative data between the HOBO pressure transducer and Arduino sensors. (A) temperature and (B) stage between August 23rd and September 5th ,2019; (C) temperature and (D) stage between September 25th and September 29th, 2019.

A comparison of the temperature measurement collected by the pressure transducer, which was installed in the water, and the Arduino temperature sensor indicated that the Arduino-based temperature sensor reads at ~ 2°C higher (Figure 4.1 A and 4.1 C). Both sensors depicted a

decrease in water temperature from late afternoon to early morning and increased during the day. The peak in temperature was recorded at around 17:00 o'clock and reached the lowest point at 7:00 o'clock every day. Overall, both sensors showed the same trends, except one peak that the Arduino sensor detected between 23:16 o'clock on August 25th to 00:50 o'clock on August 26th.

Estimate of Streamflow

The estimate of streamflow was carried out by constructing a separate rating curve for each creek. Stage measurements and stream velocity were obtained for Five Mile Creek, Willow Brook, Bentley Brook, and Hardscrabble Brook under different flow conditions. Stage-discharge relationships were developed using a quadratic equation fit through the data points by forcing the regression to go through zero (Figure 4.2).

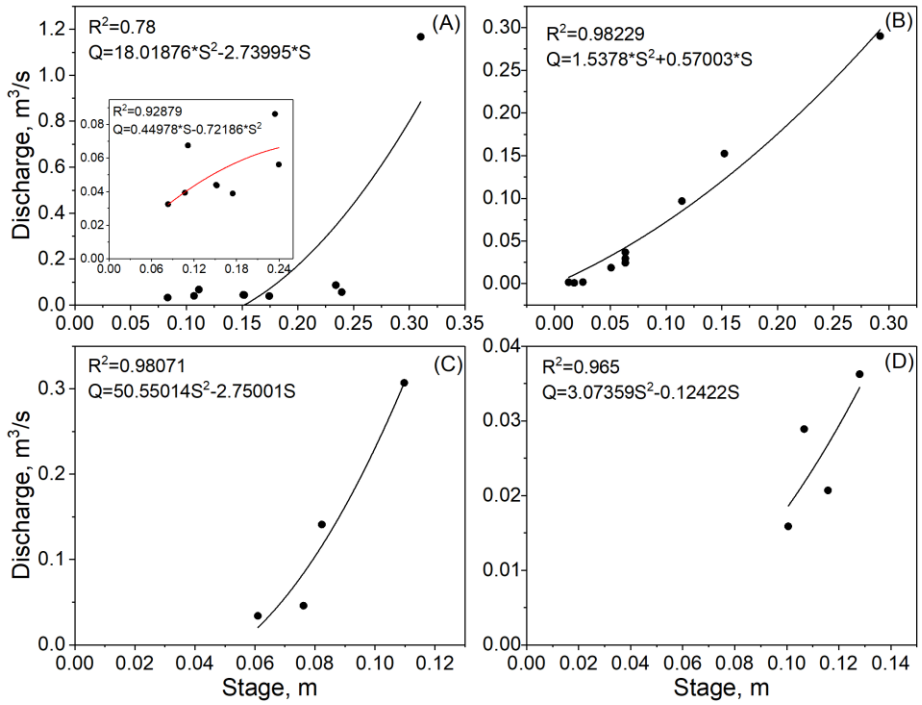

Figure 4.2: Stage-discharge relationship in (A) Five Mile Creek, (B) Willow Brook, (C) Bentley Brook, and (D) Hardscrabble Creek.

For Five Mile Creek, nine measurements were made between May 21st and October 10th, 2019. The cross-sectional areas of Five Mile Creek ranged from 0.27 m^2 to 1.11 m^2; streamflow varied from 0.03 m^3/s to 1.17 m^3/s. The statistical relationship for whole dataset between stage and streamflow had a coefficient of determination, R^2, of 0.78 (Figure 4.2 A).

For Willow Brook, fourteen measurements were collected on eight different days between May 21st to October 10th, 2019. The sampling location is a double culvert and on drier days (May 30th and October 10th), there was flow only in one of the culverts. Over the study, cross-sectional areas measurements for Willow Brook ranged from 0.08 m^2 to 0.38 m^2, and streamflow ranged from 0.02 m^3/s to 0.64 m^3/s. The rating curve had a coefficient of determination, R^2 of 0.99 (Figure 4.2 B).

Bentley Brook and Hardscrabble Creek were measured only four times (between May 21st to June 13th, 2019). The cross-sectional areas and streamflow of the creeks were very similar and ranged from 0.04 m^2 to 0.26 m^2 and 0.06 m^2 to 0.28 m^2, respectively for area and from 0.03 m^3/s to 0.31 m^3/s and 0.02 m^3/s to 0.04 m^3/s, respectively for streamflow. The rating curve for Bentley Brook had a coefficient of determination of 0.98 (Figure 4.2 C). For Hardscrabble, the statistical relationship between stage and streamflow had a coefficient of determination of 0.965 (Figure 4.2 D).

Hydrologic Response of Five Mile Creek

The custom-built multi-parameter unit was deployed in Five Mile Creek intermittently between June 6th and October 31st, 2020. All the data retrieved from custom-built multi-parameter unit is presented in the figures below, grouped by deployment dates: June 4th -5th (Figure 4.3 A),

August 14th - 23rd (Figure 4.3 B), August 27th - September 5th (Figure 4.3 C), and September 25th - 29th (Figure 4.3 D). Using the rating curve for Five Mile Creek, the stage data recorded by the ultrasonic sensor was used to estimate the discharge. The stage measurements obtained by the ultrasonic sensor had numerous false readings, which were removed from the dataset. At the beginning of the monitoring (June-July 2019), the sensor unit was powered by four size-D batteries and the unit lost power after a few days. Some of the false readings during this period were attributed to insufficient power. For example, after the first 30 hours from June 4th to June 5th, data were discarded since it repeatedly gave a depth of 33 cm. To solve the power problem, a solar panel was added to the system, which provided continuous power supply. After the solar panel was added, the false readings of the ultrasonic sensor substantially decreased, although they continued to occur periodically unrelated to a specific condition.

The first testing period (Figure 4.3 A) was over a day, but it captured a rain event on June 4th. Before and after the rain event, the baseflow was around 0.0566±0.00047 m^3/s (average discharge ± standard deviation). A cumulative precipitation of 2.5 mm produced a peak of 0.059 m^3/s. Three consecutive rain events in August with cumulative precipitation of 15.8 mm, 19.1 mm, and 25.2 mm resulted in a short-lived peak discharge of 3.05 m^3/s during the first event and a peak discharge of 2.21 m^3/s, with sustained high flow between 1.59 and 2.21 m^3/s for over an hour (Figure 4.3 B). Cumulative precipitation of 14.7 mm and 32.8 mm on August 28-29, 2019 and September 2, 2019 produced peak flow of 0.066 m^3/s and 0.067 m^3/s, respectively. Peak in discharge was not detected at the end of September (Figure 4.3 D), which is consistent with the lack of the precipitation during the second half of the month. In August, after three consecutive days of rainfall the baseflow of the Five Mile Creek was 0.054±0.0043 m^3/s. The

lowest baseflow was estimated in September with an average and standard deviation of 0.036±0.0023 m^3/s.

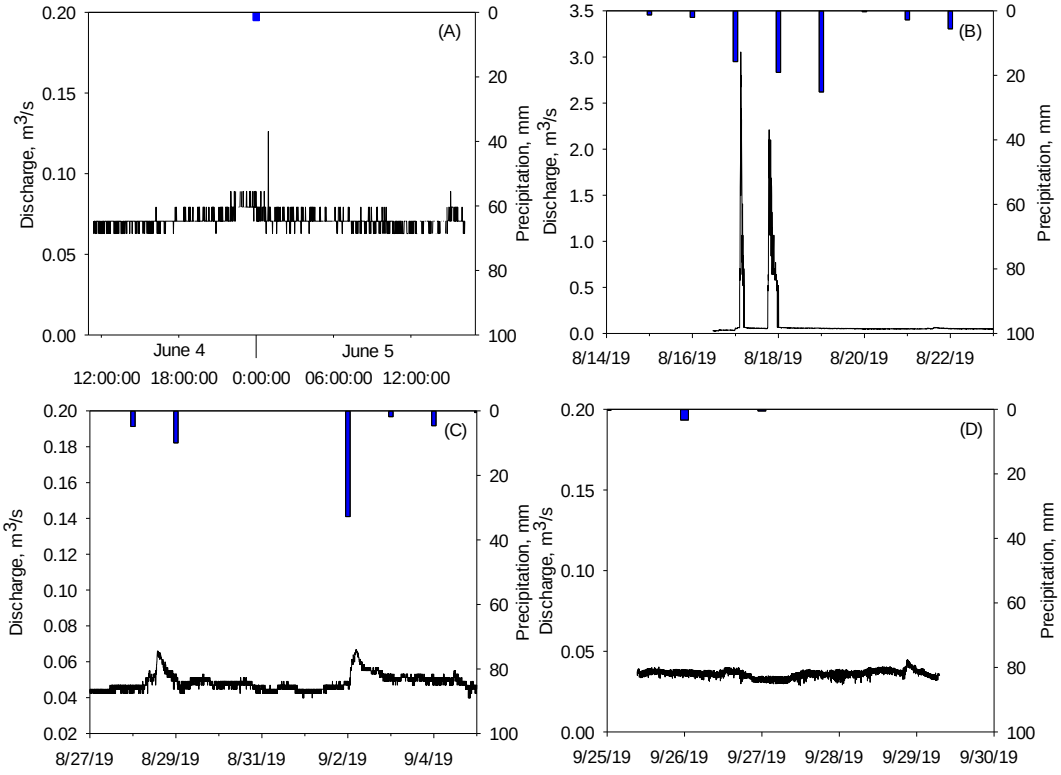

Figure 4.3: Hyetograph and Hydrograph for (A) June 4th -5th, (B) August 14th - 23rd, (C) August 27th - September 5th, and (D) September 25th -29th. Blue bars represent the total daily precipitation (mm) and black lines represent calculated stream discharge (m^3/s).

Physical Parameters

The custom-built multi-parameter unit continuously measured temperature, pH, and DO. Data retrieved from the Arduino box from June 4th - 5th, August 16th - August 21st, and August 23rd - September 4th are grouped and discussed below.

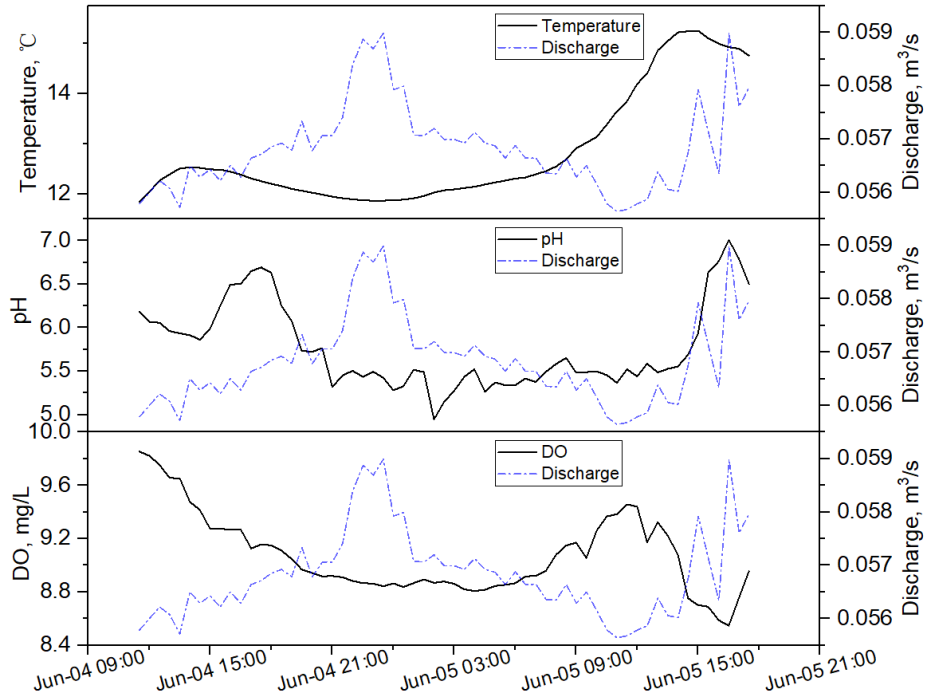

Figure 4.4: Temperature, pH, and DO data for June 4th to 5th. Blue dot and dash lines represent calculated stream discharge(m^3/s).

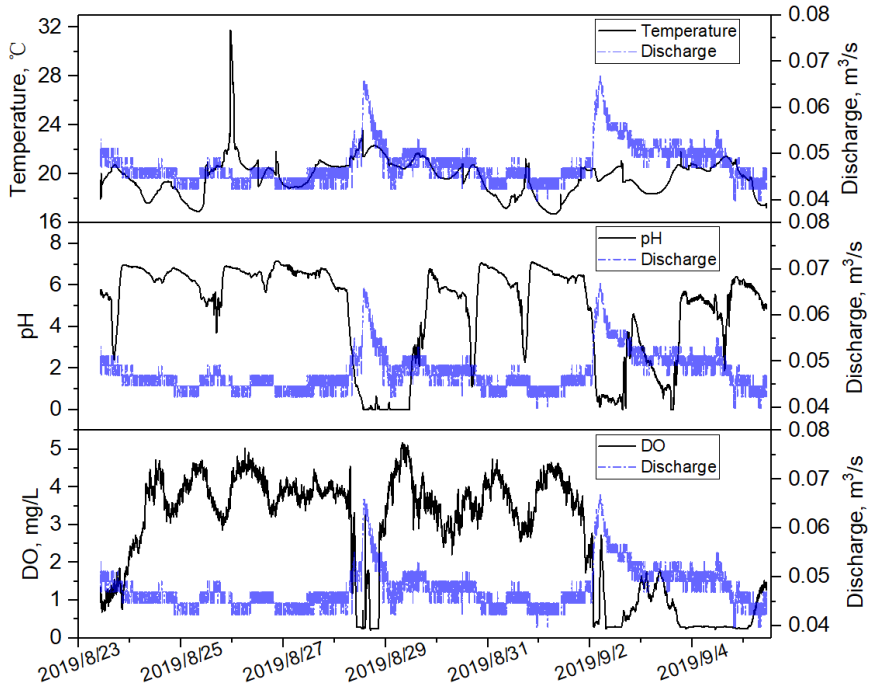

Figure 4.5: Temperature, pH, and DO data for August 23rd to September 4th. Blue dot and dash lines represent calculated stream discharge(m^3/s) information.

The sensor unit depicted diurnal variation in temperature and DO (Figure 4.4 and 4.5). Diurnal temperature fluctuations during baseflow were between 2.0-3.1°C. Temperature generally decreased during high flow events. DO concentrations were between 80% and 100% saturation in June with values ranging between 8.5 mg/L and 10.6 mg/L (Figure 4.4). Much lower DO concentrations were measured in August, between 3-5.2 mg/L, corresponding to 35% - 55% percent saturation (Figure 4.5). Over a single day, the highest DO reading was observed at noon, and the lowest during the night. The DO probe completely fouled during two high flow events in August (Figure 4.5).

The pH measurements were less stable compared to the measurements for temperature and DO. The pH was in the range of 6.2 to 7.9. However, sudden decreases in pH values were observed with sudden change in temperature.

Discussion

Applicability of the Custom-Built Multi-Parameter Sensor Unit

The unit successfully captured the variation in the flow in Five Mile Creek. A total of five high-flow events with different intensities were recorded. The two-week comparison between the ultrasonic sensor and the HOBO pressure transducers revealed that the pressure transducers were more susceptible to false readings due to shift in position during high-flow events. The pressure transducer was deployed at the bottom of the creek, tied to the pipe housing the sensors, just touching the sediments. Five Mile creek exhibits considerable variability in flow during the year. The creek responds very quickly to inputs from the watershed and during high flow

the turbulence might have lifted the HOBO pressure transducer and caused it to drift with the flow to the extent of the cord with which it was connected. Therefore, during high flow the discrepancies were even larger. The ultrasonic sensor provided more accurate readings and appeared to be more reliable during high-flow evens. The stage measurement with the ultrasonic sensor is a non-obstructive method advantageous to the traditional approaches of measuring water level with weir as it does not require special installation and maintenance, does not result in buildup of sediments and debris, and is more reliable at high flows.

The temperature sensor had the best performance among the three water quality sensors. It successfully captured diurnal variations. There was a constant discrepancy of about 2°C between the readings of the temperature sensor built in the HOBO pressure transducer and the temperature sensor used in the multi-parameter sensor unit. The temperature sensor in the multi-parameter sensor unit was measuring higher temperature all the time. This difference might be coming from the fact that the Arduino sensor was positioned higher in the creek while the sensor embedded into the HOBO pressure transducer was close to the surface sediments. A calibration error for one of the units is also plausible. Overall, the temperature and stage readings of the sensor unit were reliable and can be used for future monitoring efforts. On cost basis, the total cost of the temperature sensor and the ultrasonic sensors is 18% of the cost of a pair of pressure transducers.

The pH sensor performed well under low flow conditions but was unstable during high flow events. Under low flow, consistent decreases in pH were noted at the same time of the day (Figure 4.6), which cannot be explained either by the standard change in pH with water temperature or by the photosynthetic activities in the stream. The pH represents the logarithmic

change in the activity of the hydrogen ion in water. The ion product of water, k_w, under standard conditions (1 atm and 25°C) is 10^{-14}. The formation of the hydrogen ion is an endothermic process and the change in water temperature would change the value of k_w and thus, the measured pH (Brezonik and Arnold 2011). The k_w decreases with the decrease in temperature, which will result in higher pH reading. The relationship is reversed at higher temperature. For the temperature range of 15 - 30°C observed in Five Mile Creek during the summer, the variation in the readings at pH = 7 would be between 7.17 and 6.92, respectively. The variation in pH observed on the field was up to 4 pH units, which means that stream water temperature alone cannot explain it. If the change in pH was driven by photosynthesis, the process in which carbon dioxide (CO_2) is utilized by algae and oxygen is produced, the pH would follow a diurnal pattern of an increase during the day and a decrease during the night. This pattern has been observed in both headwater and larger river systems (de Montety et al., 2011; Hayashi et al., 2012; Pu et al., 2017). However, the diurnal pattern is not consistent with the afternoon decreases in pH recorded at Five Mile Creek.

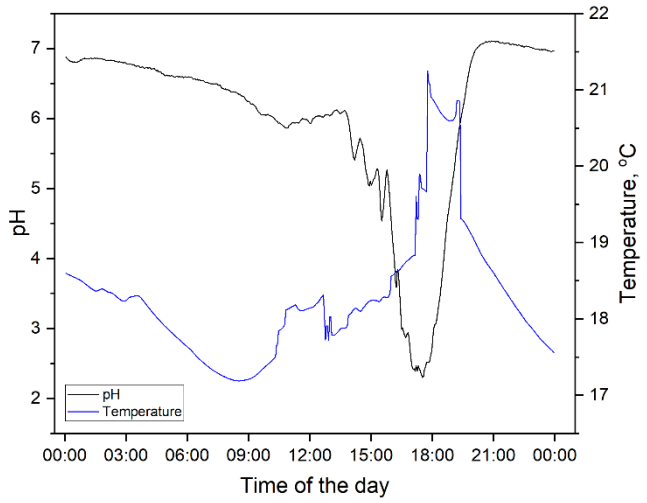

Figure 4.6: Daily variation of pH and temperature in Five Mile Creek for a representative day in August.

The recurring daily decrease at Five Mile Creek appeared at discrete times in the afternoon, which could be attributed to the shading effect of a large tree southeast of the sensor location. To determine the effect of the tree, a shading analysis was performed for a representative day in August, which determined that the box housing the multi-parameter sensor unit had the highest exposure to sun between noon and sunset (Figure 4.7), which coincides with the time of rapid decrease in pH (Figure 4.6). Therefore, the recurring decreases in pH during the day are most probably a result of overheating the electronics. The recovery of the pH sensor overnight affirms that the errors are reversible and can be eliminated. Further laboratory and field tests are underway to determine how to predict and compensate for the decreases in pH on the field. Under high flow, the pH sensor repeatedly malfunctioned, and its recovery was prolonged. Recalibration between deployments has been done and have improved the readings of the pH sensor. In the future, exchange of the sensors should be explored as a recovery tool.

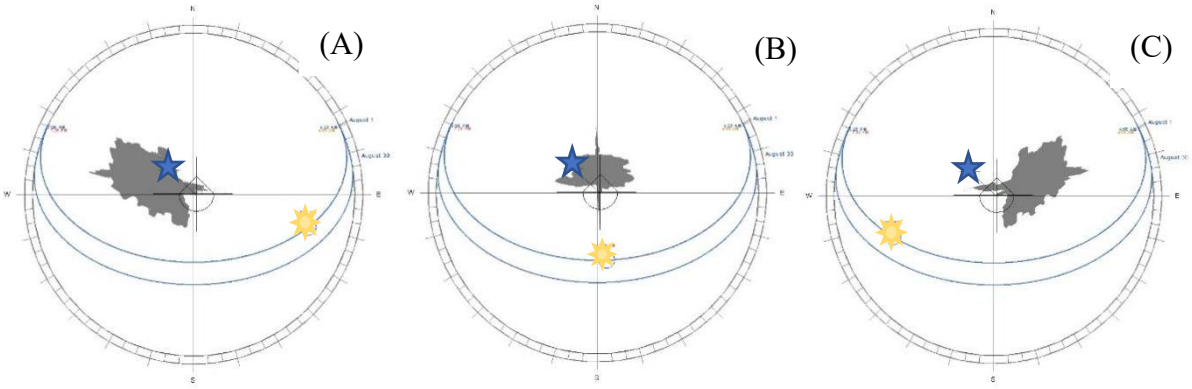

Figure 4.7: Shading of the multi-parameter sensor unit at A) 9:00 am, B) 12:00 pm, and C) 3:00 pm for a representative day in August 2019. The tree is located at the center of the circle. The multi-parameter sensor unit is designated with a blue star.

The DO sensors captured the natural diurnal pattern in response to solar heating and photosynthetic activities. Despite following manufacturer's calibration protocol, the DO

concentrations in August were substantially below saturation. The month of August had a record of rainy days (Figure 4.8). Daily precipitation occurred between August 7th, 2019 and August 11th, 2019 that totaled to 57.7 mm, followed by another precipitation series between August 13th, 2019 and August 22nd, 2019, which brought 84.3 mm of precipitation. The prolonged precipitation period most probably reconnected hydrologic pathways that carried lower DO concentrations. I am not aware of any direct combined stormwater discharges into the creek which could bring organic contamination into the stream and result in decreases in DO, but it should be noted that the area does not have a centralized sanitary sewer system and relies on septic systems. During the high-intensity rain events on August 28th-29th, 2019 and September 2nd, 2019 (Figure 4.3) the membrane on the DO sensor most probably fouled because of increased sediment loading. The probe was able to recover after the first event (August 28th-29th) but required cleaning and calibration after the second event (September 2nd).

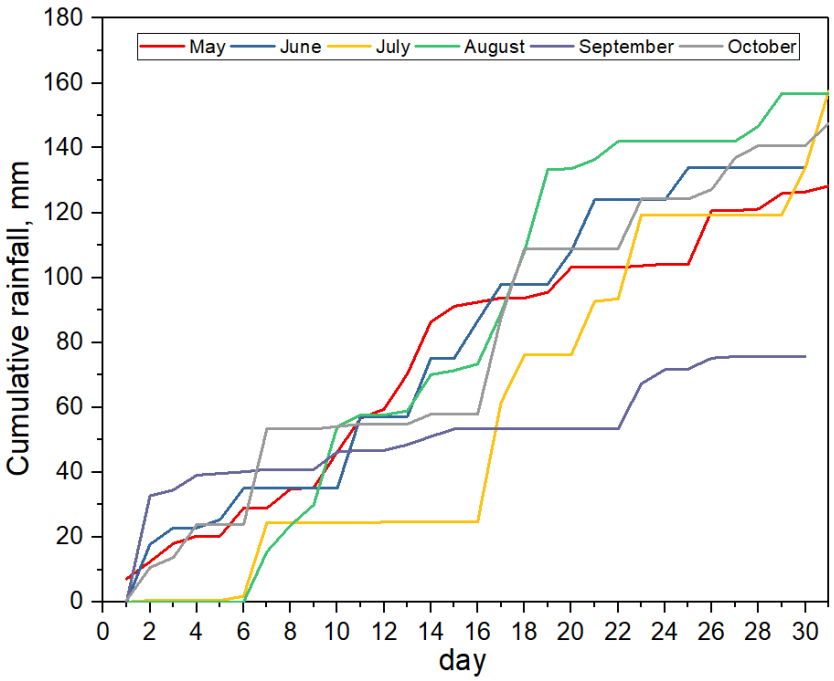

Figure 4.8: Cumulative rainfall for the village of Skaneateles for May, June, July, August, September, October 2019.

Streamflow Estimates

Different stream conditions were captured during the high frequency monitoring periods in June, August, and September of 2019, which allowed the development of the rating curves for Five Mile Creek, Willow Brook, Hardscrabble Brook, and Bentley Brook. All the rating curves showed statistically significant relationships. To test the prediction power of the rating curves for Five Mile Creek, Willow Brook and Bentley Brook, the respective equations were used to calculate the flow in the creek using the stage measurements. Despite the statistically good correlation, the power relationship for Five Mile Creek, which is typically used for rating curves in hydrology, consistently under-predicted the creek flow below 0.05 m^3/s with difference between three to four orders of magnitude and overpredicted the high flow with about 100%. The rating curve for Five Mile Creek had one high flow data with stage of 0.31 m and streamflow of 1.17 m^3/s on June 20th, 2019. This data point appeared to be highly influential as it changed the statistical relationship substantially. The lack of additional data points at high flow impeded the applicability of the power rating curve over a broad range. A forced-though-zero quadratic equation was a better predictor of the high flow in the creek. The rating curves for both Willow Brook and Bentley Brook had good predicting capability for the range they were developed.

Repeated discharge rating of all the creeks is necessary because the stage-discharge relationship is not static over a long period. The creeks had muddy bottom, erosion and sediment deposition may have altered the cross-section of the river channel, which added to the variability and inaccuracy of the relationships developed here. Willow Brook was an exception, which was gauged at a culvert. In addition, Bentley Brook and Hardscrabble Brook were gauged only four

times during 2019. The goal is to continuously update the rating curves as more data is collected in subsequent years.

Hydrologic Response of Five Mile Creek

The measurements of stream stage were responsive to both short-term precipitation patterns and long-term seasonal changes. The cumulative monthly precipitation during the monitoring period (May to October) shows that September was the driest month with total precipitation of 75.7 mm (Figure 4.8). August was dry during the first 10 days of the month. Series of rain events brought about 84.3 mm of precipitation between August 13th and August 22nd, which coincided with the time of deployment of the sensor unit. Both June and August had higher than normal cumulative precipitation (http://climod2.nrcc.cndornell.edu/), which resulted in higher baseflow during these months – 0.056 m^3/s in June and 0.054 m^3/s in August (average data). Baseflow in September was estimated to be 0.036 m^3/s, on average.

The stream flow responded to all high precipitation events. The cumulative daily precipitation does not correlate with the peak flow in Five Mile Creek. For instance, a 32.8 mm precipitation on September 2nd, 2019 has a corresponding peak flow of 0.067 m^3/s, while 84.3 mm precipitation resulted in a discharge of 3.05 m^3/s on August 16th, 2019. I attributed this to the antecedent conditions (period without precipitation between precipitation events) before the events and to the storage capacity of a wetland in the upper part of the watershed. The antecedent dry periods (ADP) were calculated for each of the events. The events on June 4th and August 16th and 17th had an ADP = 1. As for August 28th the ADP = 6, and for September 2nd, the ADP = 4. ADP is inversely proportional to soil moisture and the storage capacity of the

soil. The shorter the ADP, the quicker the response of the creek to the rain event and the higher the peak because the soil is already saturated from prior rain event and does not have enough storage capacity. Therefore, the comparable precipitation on August 16th and September 2nd produced different hydrographs. Overall, the watershed appears to be well drained at precipitation events above 2.5 mm each, which would result in quick export of material.

CHAPTER 5 Nutrients Behavior in Nine Creeks in Skaneateles Lake Watershed

Results

A wide range of concentrations were observed in the organic carbon, nitrogen, and phosphorus species in the nine creeks that were monitored from August 2018 to February 2020. Trends and relationships were developed for the whole dataset and for individual creeks to understand the behavior of the nutrients.

The Effect of Physical Characteristics of the Watershed on Nutrient Levels

Carbon, nitrogen, and phosphorus data were analyzed with respect to the physical parameters of the watersheds, including stream order, mean basin slope, watershed area, and watershed land use. These analyses aimed to determine how the physical features of the watershed influence the concentration of the studied nutrients.

Stream Order

The stream order is a geomorphological characteristic of streams that reflects the branching of the stream and can be potentially linked to the size of the stream and its watershed. For the following analysis, stream order was determined manually from existing USGS hydrological maps (Table 5.1).

Table 5.1: Stream order for study creeks

Creek Name	Stream Order
Fisher Brook	1st
Bentley Brook	2nd
Dowling Creek	2nd
Hardscrabble Brook	2nd
Mile Point Creek	2nd
Five Mile Creek	3rd
Glen Cove	3rd
Ten Mile Creek	3rd
Willow Brook	3rd

Overall, the highest average concentration of TOC, TN, NO_x, and of all P species were found in the first order stream (Figure 5.1). It should be noted that there is only one stream which is first order, Fisher Brook. For the TOC species, the average concentration decreased with an increase in stream order. The first order stream had an average TOC concentration of 6.36±1.85 mg/L. This pattern did not hold for DOC, where the highest mean concentration of 5.45±2.20 mg/L was in the second order streams. Like carbon species, the highest mean TN and NO_x occurred in the first order stream (TN of 3.7±1.31 mg/L, and NO_x of 2.92±1.43 mg/L) but there was no apparent pattern with the increase in stream order. For NH_4^+, the second order streams had the highest mean concentration of 0.025±0.033 mg/L. For phosphorus species, the highest average concentration was always observed in the first order stream (TP = 0.38±0.46 mg/L, TDP = 0.11±0.068 mg/L, and SRP = 0.10±0.065 mg/L). Second and third order streams had similar concentrations.

Basin Slope

The relationship between basin slope and mean nutrient concentration was examined to identify

any potential influence of the length of the hydrological flow path and connectivity. Both TOC and DOC showed a statistically significant negative correlation with mean basin slope (Figure 5.2, TOC: $R^2 = 0.33$, $p = 0.1$; DOC: $R^2 = 0.47$, $p = 0.04$). TOC concentrations decreased 1 mg/L for every 6.6% increase in basin slope. The DOC concentrations showed a decrease of 1 mg/L for every 5.2% increase in basin slope. Except for NH_4^+, the concentration of N and P species increased with an increase in basin slope, although these increases were not statistically significant (Figure 5.2).

Watershed Area

The correlation between nutrient concentrations in streams and their corresponding watershed areas was explored (Figure 5.3). For nitrogen species, both TN and NO_x showed a positive correlation with the watershed area. This correlation was statistically significant for TN ($p = 0.07$), while for NO_x this pattern showed no statistical significance ($p = 0.5$). Meanwhile, NH_4^+ and P species were negatively correlated to the watershed area. These relationships were not statistically significant ($p = 0.4 - 0.7$).

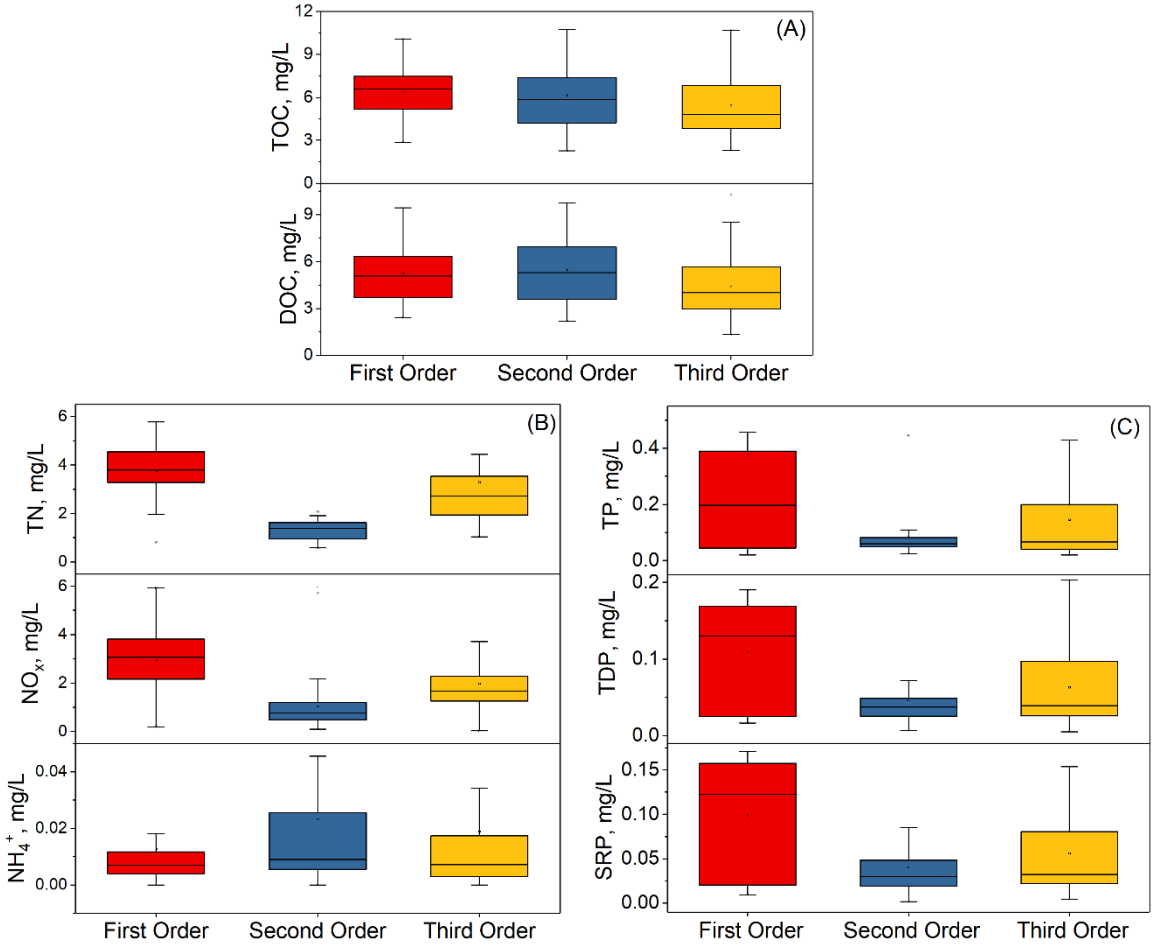

Figure 5.1: Box and whisker plots of (A) organic carbon, (B) nitrogen, and (C) phosphorus species by stream order. The boundary of each box represents a quartile (bottom of the boundary denotes lower quartile, upper of the boundary denotes the upper quartile); the line in each box represents the median; the average is denoted by small squares in the boxes; whiskers symbolize 10th and 90th percentile; the asterisk (*) identifies statistical outliers.

The organic carbon species appeared to be strongly and negatively correlated with the watershed area (TOC: $R^2 = 0.92$, $p = 0.0005$; DOC: $R^2 = 0.92$, $p = 0.0006$) with a 1 mg/L increase of TOC or DOC concentrations for every 0.7 km^2 decrease in basin area. The two creeks that deviated from this relationship and were excluded from the regression line were Five Mile Creek and Bentley Brook. These two creeks have the largest watersheds, but they are the only creeks with open wetland areas comprising 6.4% and 13.5%, respectively, from the total watershed area. The other seven creeks had zero percent wetland area.

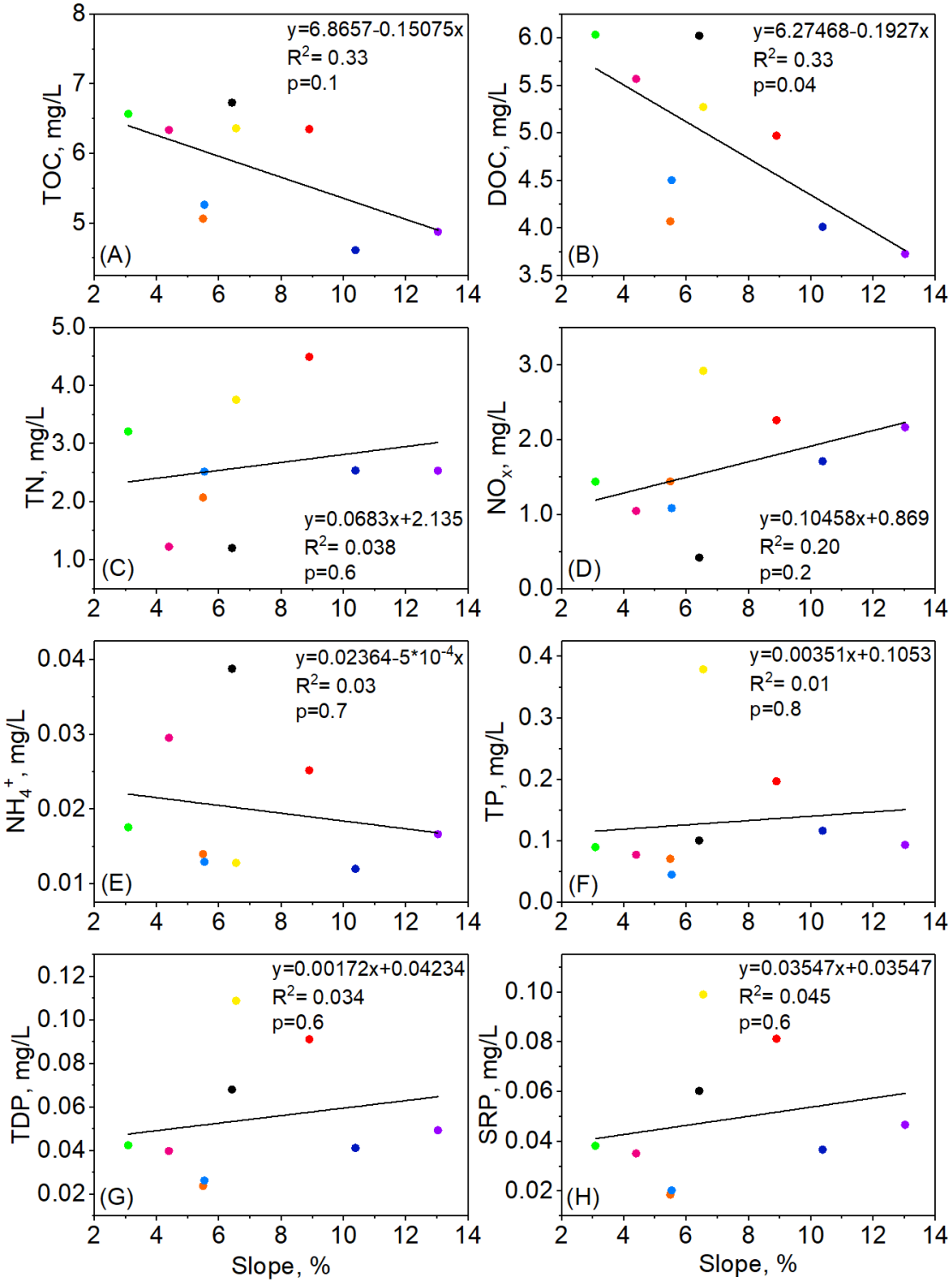

Figure 5.2: Correlations between watershed slope and nutrient species: (A) TOC, (B) DOC, (C) TN, (D) NO_x, (E) NH_4^+, (F) TP, (G) TDP, (H) SRP for Bentley Brook (green), Dowling Creek (pink), Fisher Brook (yellow), Five Mile Creek (red), Glen Cove (dark blue), Hardscrabble Brook (blue), Mile Point Creek (black), Ten Mile Creek (purple), and Willow Brook (orange). Black line represents linear regression between two parameters.

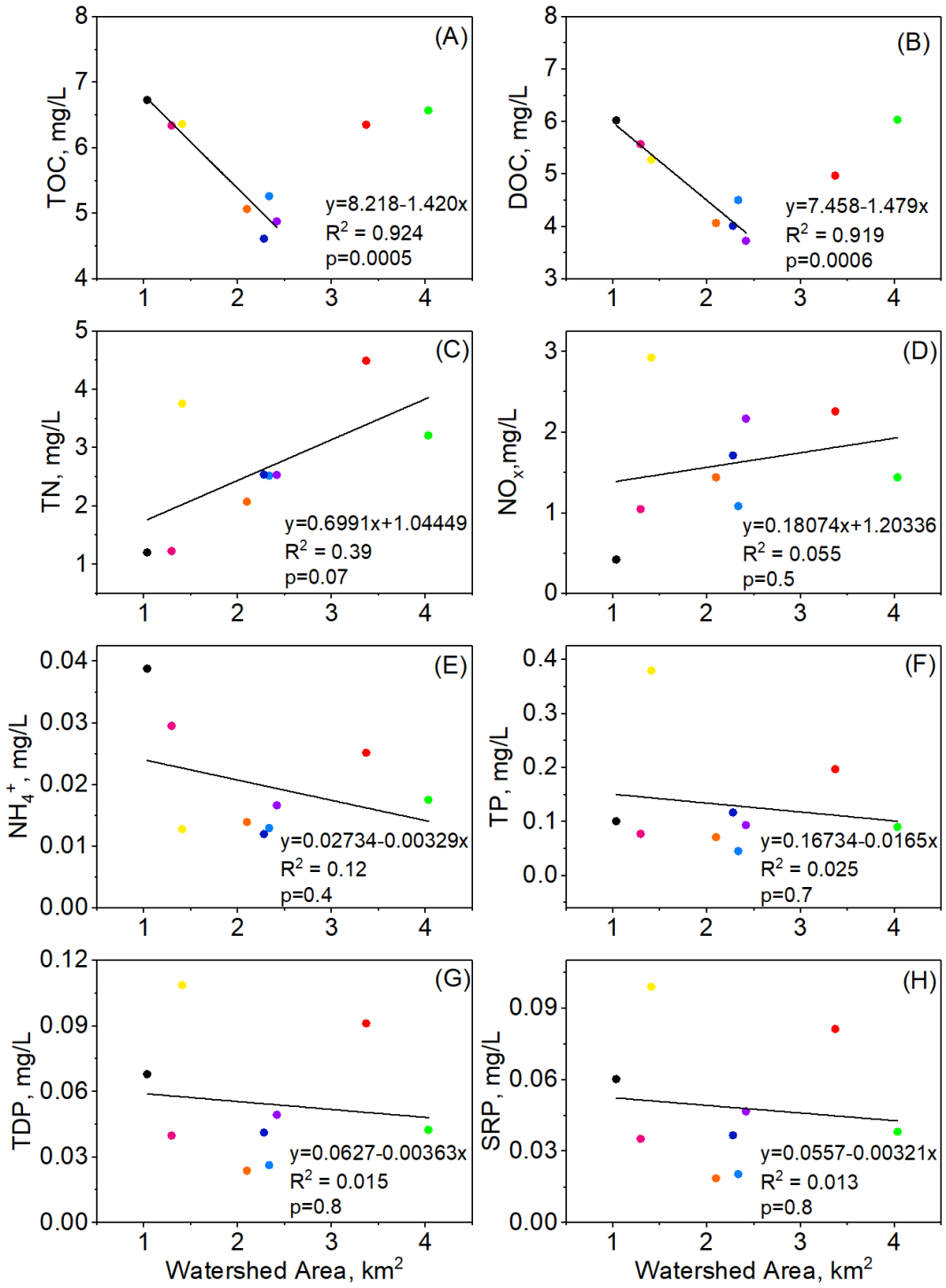

Figure 5.3: Correlations between watershed area and nutrient species: (A) TOC, (B) DOC, (C) TN, (D) NO_x, (E) NH_4^+, (F) TP, (G) TDP, (H) SRP concentrations for Bentley Brook (green), Dowling Creek (pink), Fisher Brook (yellow), Five Mile Creek (red), Glen Cove (dark blue), Hardscrabble Brook (blue), Mile Point Creek (black), Ten Mile Creek (purple), and Willow Brook (orange). Black line represents linear regression between two parameters.

Nutrient Concentrations by Creek

In this part, carbon, nitrogen, and phosphorus data from all creeks were integrated and compared to assess the geochemical behavior of each nutrient.

Carbon Species

The mean TOC concentrations for all tributaries although variable, were within the same order of magnitude and did not show statistical difference (Figure 5.4, p=0.172-1.0). They ranged from 4.61±1.33 mg/L in Glen Cove to 6.73±2.03 mg/L in Mile Point Creek. The two highest individual TOC concentrations were 13.43 mg/L at Dowling Creek and 10.72 mg/L Hardscrabble Brook. The peak at Dowling Creek occurred on July 17th, 2019 when a cumulative daily precipitation of 36.8 mm was recorded, and the elevated value at Hardscrabble Brook occurred on July 25th, 2018 when a cumulative daily precipitation of 35.6 mm was recorded. The lowest individual TOC concentration of 2.27 mg/L was observed on March 14th in Dowling Creek when no precipitation was recorded.

Like the mean TOC concentrations, mean DOC concentrations did not vary considerably among the creeks and ranged between 3.73±1.92 mg/L (Ten Mile Creek) and 6.03±2.10 mg/L (Bentley Brook). There was also no statistical difference between the DOC concentrations (p=0.079-1.0). The highest individual DOC value was 13.20 mg/L, measured in a sample collected from the Dowling Creek, on the same day as the highest TOC concentration (July 17th, 2019). The lowest individual DOC, however, was observed at Five Mile Creek on July 19th, 2018, which was a day without a precipitation event.

Nitrogen Species

Mean TN concentrations varied among tributaries (Figure 5.5A). The tributaries with the

highest average TN concentrations were Five Mile Creek (4.49±2.88 mg/L) and Fisher Brook (3.76±1.31 mg/L). Mile Point and Dowling Creek had the lowest average TN at 1.20±0.39 mg/L and 1.23±0.86 mg/L, respectively. Statistically, only Five Mile Creek had significantly higher TN concentration than Dowling Creek (p=0.005) and Mile Point Creek (p=0.007). The highest individual TN concentration was observed at Bentley Brook (11.90 mg/L) on July 17th, 2019, when the cumulative daily precipitation was 36.8 mm. The lowest individual TN concentration was observed at Dowling Creek (0.58 mg/L) on February 5th, 2020, when no precipitation was recorded.

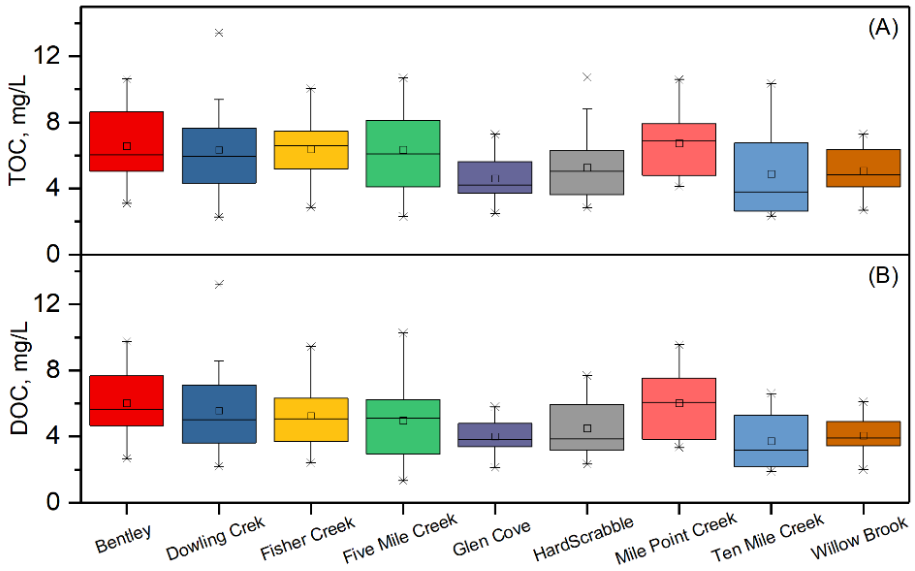

Figure 5.4: Box and Whisker plots for average concentrations of: (A) TOC and (B) DOC in the nine tributaries. The boundary of each box represents a quartile (bottom of the boundary denotes lower quartile, upper of the boundary denotes the upper quartile); the line in each box represents the median; the average is denoted by small squares in the boxes; whiskers symbolize 10th and 90th percentile; the asterisk (*) identifies statistical outliers.

Noticeable variation exists in the mean NO_x concentrations (Figure 5.5B). The highest average NO_x concentrations were calculated for Fisher Brook (2.92±1.43 mg/L) and Five Mile Creek (2.26±1.72 mg/L). The lowest average NO_x concentration was at Mile Point Creek (0.42±0.28

mg/L), which was statistically lower than Five Mile Creek ($p<0.001$), Fisher Brook ($p< 0.001$), Glenn Cove ($p=0.017$), and Ten Mile Creek ($p=0.002$). The highest individual NO_x concentration of 7.17 mg/L was observed at Five Mile Creek on October 4th, 2018, when the cumulative daily precipitation was 0.3 mm. The lowest individual concentration of 0.03 mg/L was also at Five Mile Creek, on June 11th, 2019 when cumulative precipitation of 22.1 mm was recorded.

Mean NH_4^+ concentrations were consistently low among all tributaries (Figure 5.5C), and there was no statistical difference between the NH_4^+ concentrations ($p=0.147$-1.0). They ranged from 0.012±0.02 mg/L in Glen Cove to 0.0388±0.05 mg/L in Mile Point Creek. The highest individual concentration (0.27 mg/L) was measured at Five Mile Creek, and lowest (0.000084 mg/L) individual concentration was measured at Fisher Brook. The highest individual value was observed on June 16th, 2019, a day with a cumulative precipitation of 11.4 mm; while the lowest individual value was on August 17th, 2019 with a cumulative precipitation of 15.7 mm. Many NH_4^+ concentrations were below the detection limit and are not reported here.

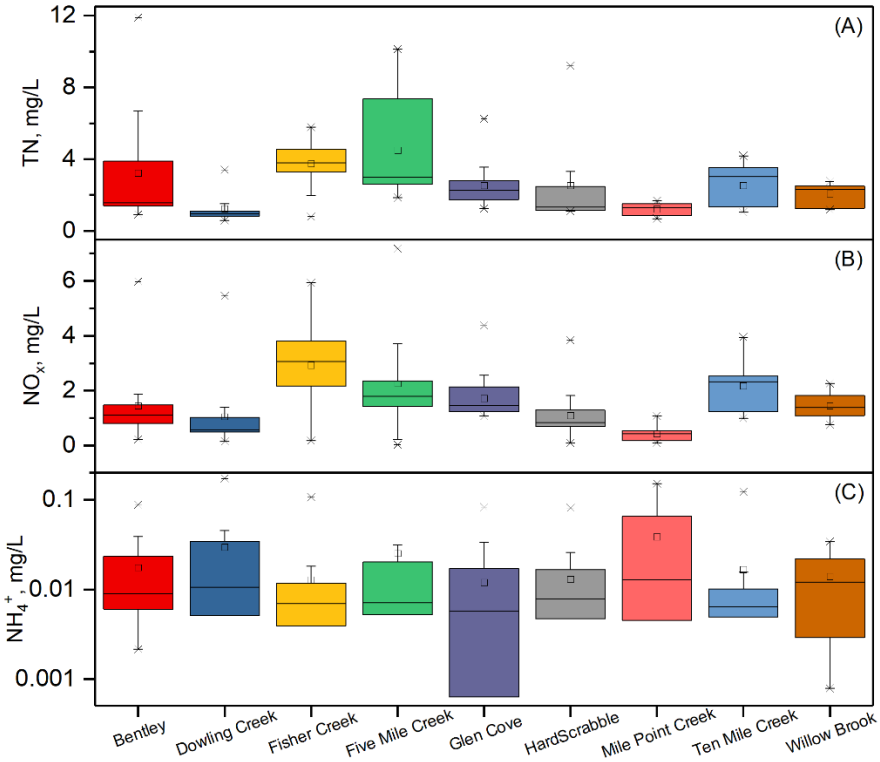

Figure 5.5: Box and Whisker plots for average concentrations of: (A) TN, (B) NO_x, and (C) NH_4^+. The boundary of each box represents a quartile (bottom of the boundary denotes lower quartile, upper of the boundary denotes upper quartile); the line in each box represents the median; the average is denoted by small squares in the boxes; whiskers symbolized 10th and 90th percentile; the asterisk (*) identifies statistical outliers.

Phosphorus Species

The mean TP concentrations showed great variability among the creeks (Figure 5.6A). Nevertheless, there was no statistical difference between TP concentrations in the studied creeks (p=0.854-1.0). The lowest average concentration was detected at Hardscrabble Brook (0.046±0.012 mg/L). The creeks with the highest average TP concentrations were Fisher Brook (0.38±0.46 mg/L) and Five Mile Creek (0.20±0.19 mg/L). The highest individual TP concentration of 1.58 mg/L was observed at Fisher Brook on August 17th, 2019 when the cumulative daily precipitation was 15.7 mm. The lowest individual TP concentrations were

observed at Five Mile Creek and Fisher Brook of 0.020 and 0.021 mg/L, respectively on September 14th, 2018 and August 31st, 2018, on days without a recorded precipitation.

The average TDP and SRP shared the same spatial distribution (Figure 5.6B and 5.6C). The highest average TDP and SRP were calculated at Fisher Brook at 0.109±0.068 mg/L and 0.0989±0.065 mg/L, respectively. The lowest average concentrations for TDP and SRP were calculated at Willow Brook and were 0.024±0.016 mg/L and 0.019±0.015 mg/L, respectively. TDP and SRP concentrations were significantly different only between Fisher Brook and Willow Brook ($p=0.025$ for TDP, and $p=0.028$ for SRP) but not with the other creeks ($p= 0.075 – 1.0$). The highest individual TDP values were observed on days with precipitation, such as 0.417 mg/L at Mile Point Creek on April 28th when 3.8 mm precipitation was recorded, and 0.312 mg/L at Five Mile Creek on June 20th when 10.2 mm rainfall was recorded. The lowest individual TDP concentration of 0.0052 mg/L was observed on July 29th at Ten Mile Creek. There was no precipitation on record for that day. Like the TDP concentrations, the highest and lowest individual SRP values were observed at the same locations, on the same dates: the highest SRP were 0.398 mg/L at Mile Point Creek and 0.295 mg/L at Five Mile Creek, respectively, while the lowest was 0.0015 mg/L at Dowling Creek.

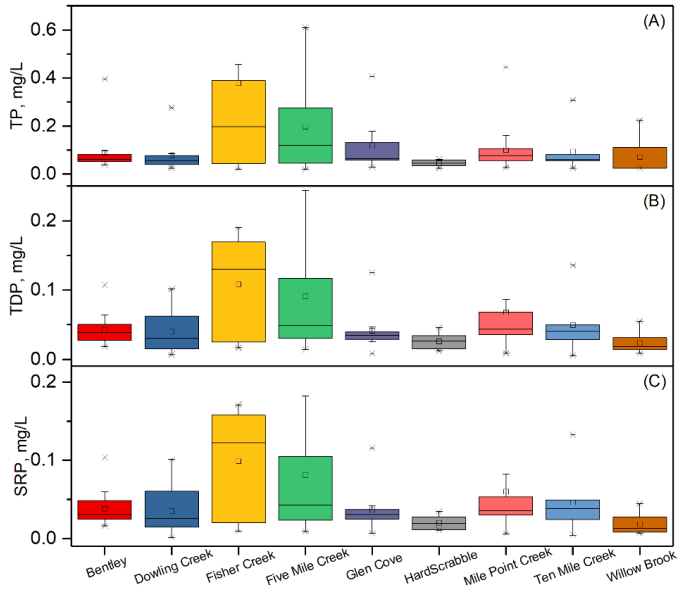

Figure 5.6: Box and Whisker plots of average concentrations of: (A) TP, (B) TDP, and (C) SRP. The boundary of each box represents a quartile (bottom of the boundary denotes lower quartile, upper of the boundary denotes upper quartile); the line in each box represents the median; the average is denoted by small squares in the boxes; whiskers symbolized 10th and 90th percentile; the asterisk (*) identifies statistical outliers.

Seasonal Change of Carbon, Nitrogen, and Phosphorus Concentration in Streams

A seasonal pattern was observed in organic carbon concentrations in all tributaries (Figure 5.7). TOC, DOC, and SOC concentrations were higher during warmer periods (summer and fall) and lower during colder periods (winter and spring) of each year. Summer SOC concentrations in 2018 were statistically significantly higher than fall ($p=0.003$) and winter ($p=0.023$). In 2019, the SOC concentrations in the fall were significantly higher than all other seasons (p ranges from <0.001 to 0.002). As for TOC and DOC, the differences were statistically significant only for 2019 (p from < 0.001 to 0.048). In 2018, the highest TOC and SOC concentrations of 6.42±2.60 mg/L and 1.52±1.09 mg/L, respectively were in the summer, while the highest DOC concentration of 5.35±1.50 mg/L was in the fall. The lowest TOC and DOC, were observed in winter with 4.93±1.01 mg/L, 4.49±0.81 mg/L, respectively, while the lowest SOC was

observed in fall with 0.31±0.18 mg/L. During 2019, the highest TOC and SOC were observed in the fall (6.91±1.78 mg/L and 1.71±1.05 mg/L), while the highest DOC of 5.73±2.38 mg/L was found in the summer. The lowest TOC, DOC, and SOC were detected during spring 2019, showing 4.30±1.12 mg/L, 3.56±0.97 mg/L, and 0.66±0.40 mg/L, respectively. The highest individual measurement of TOC and DOC both occurred in summer 2019, which was the season with the highest accumulated precipitation between summer 2018 and winter 2019 (448 mm, Table 5.2).

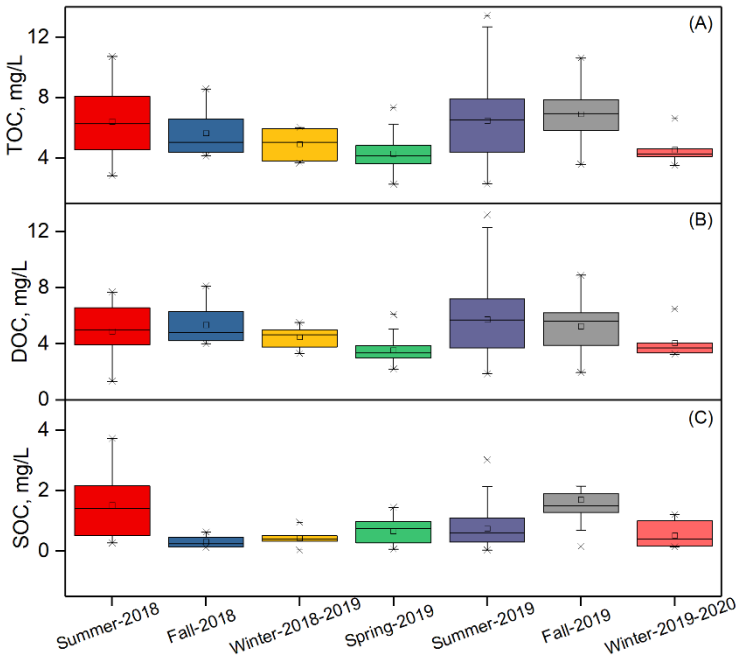

Figure 5.7: Box and Whisker plots of carbon by season: (A) TOC, (B) DOC, (C) SOC. The boundary of each box represents a quartile (bottom of the boundary denotes lower quartile, upper of the boundary denotes upper quartile); the line in each box represents the median; the average is denoted by small squares in the boxes; whiskers symbolized 10th and 90th percentile; the asterisk (*) identifies statistical outliers.

There were no apparent seasonal patterns in the distribution of the N species (Figure 5.8, p=0.148-1.0). TN and ON had similar behavior. In 2018, the highest concentrations of TN

(6.48±3.93 mg/L) and ON (1.54±0.75 mg/L) were calculated in the fall and the lowest were in the summer (2.97±0.81 mg/L for TN and 0.76±0.36 mg/L for ON), but this pattern was not sustained in 2019. In 2019, the highest TN (3.16±2.65 mg/L) and ON (1.07±1.76 mg/L) were in the summer. The lowest was in the spring for TN (1.57±0.73 mg/L) and winter for ON (0.19±0.097 mg/L). The highest single measurement of all nitrogen species appeared in the summer of 2019.

Table 5.2 Cumulative precipitation (mm) by season

Year	Season	Cumulative Precipitation (mm)
2018	Summer	265.7
2018	Fall	320.8
2018	Winter	233.4
2019	Spring	285.0
2019	Summer	448.1
2019	Fall	310.6
2019	Winter	298.7

NO_x concentrations had variable distribution with seasons (Figure 5.8B, p=0.148-1.0). The highest concentration of NO_x was in the winter of 2018 (2.7±1.57 mg/L) and the lowest was in the spring of 2019 (1.23±1.10 mg/L). Note that the distribution of all N species had similar patterns in 2019, exhibiting summer highs and winter lows. The highest single measurement of all N species appeared in the fall of 2018.

NH_4^+ concentrations appeared to have some seasonality as they were lower during cold periods and higher during warm periods (Figure 5.8C), although they were not statistically significant (p=0.176-1.0). The ammonium concentrations in the winter were the lowest compared to the rest of the year. However, the highest concentration in 2018 was during the fall (0.027±0.033

mg/L), while the highest concentration in 2019 was observed in the summer (0.034±0.079 mg/L). The highest single measurement of ammonium was observed in the summer of 2019.

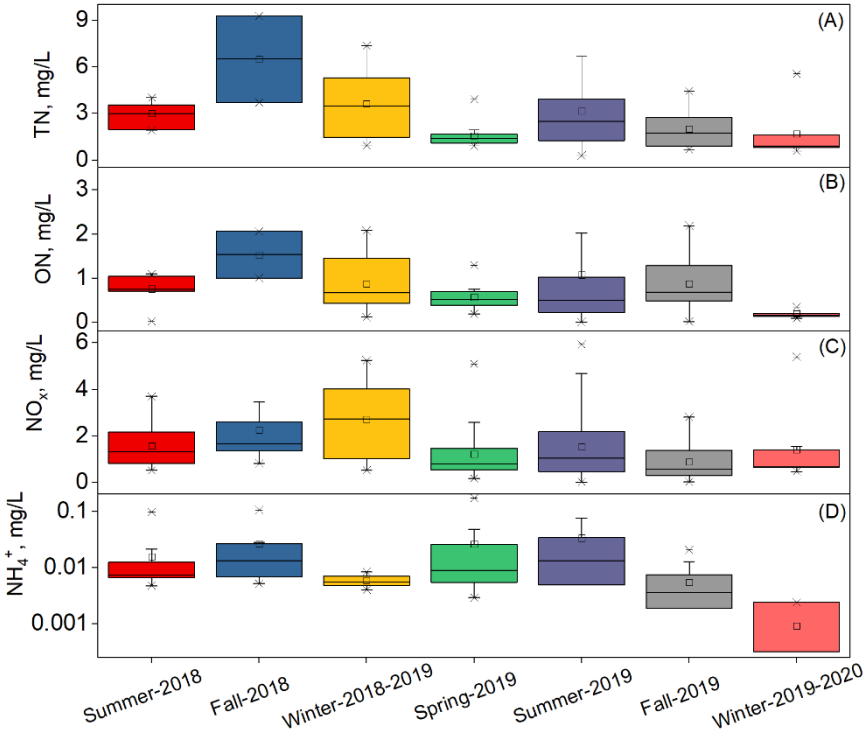

Figure 5.8: Box and Whisker plots of nitrogen by season: (A) TN, (B) NO, (C) NO_x, and (D) NH_4^+. The boundary of each box represents a quartile (bottom of the boundary denotes lower quartile, upper of the boundary denotes upper quartile); the line in each box represents the median; the average is denoted by small squares in the boxes; whiskers symbolized 10th and 90th percentile; the asterisk (*) identifies statistical outliers.

Winter and spring of each year always brought the highest concentrations in all phosphorus species (Figure 5.9). There were statistical differences in the concentrations of TDP and SRP in 2019 between spring and summer (both $p<0.001$), while there were no statistical seasonal differences for TP ($p=0.706$-1.0), and SP concentrations ($p=0.854$-1.0). In 2018, winter brought the highest average concentrations in the creeks (0.16±0.15 mg/L for TP, 0.04±0.067 mg/L for SP, 0.12±0.11 mg/L for TDP, and 0.11±0.11 mg/L for SRP), while the lowest phosphorus

concentration was measured in the fall (TP was 0.04±0.02 mg/L, SP was 0.008±0.005 mg/L, TDP was 0.03±0.02 mg/L, and SRP was 0.03±0.02 mg/L). In 2019, the highest mean phosphorus concentrations were in the spring (0.19±0.22 mg/L for TP, 0.13±0.24 mg/L for SP, 0.10±0.08 mg/L for TDP, and 0.10±0.08 mg/L for SRP), followed by winter (0.16±0.16 mg/L for TP, 0.13±0.17 mg/L for SP, 0.08±0.04 mg/L for TDP, 0.08±0.04 mg/L for SRP).

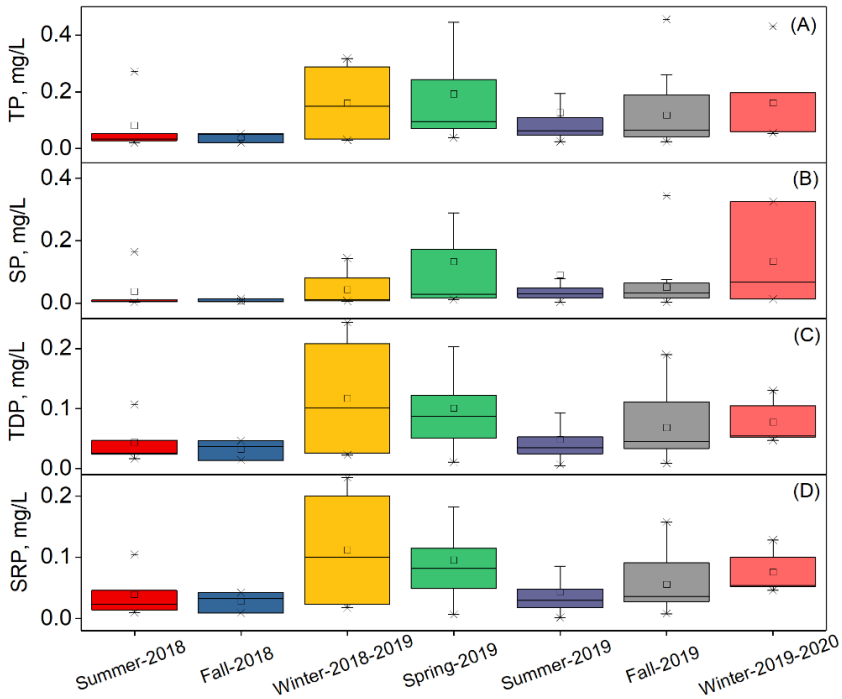

Figure 5.9: Box and Whisker plots of phosphorus by season: (A) TP, (B) SP, (C) TDP, (D) SRP. The boundary of each box represents a quartile (bottom of the boundary denotes lower quartile, upper of the boundary denotes upper quartile); the line in each box represents the median; the average is denoted by small squares in the boxes; whiskers symbolized 10th and 90th percentile; the asterisk (*) identifies statistical outliers.

Fraction of Nutrient Species

In addition to the direct laboratory measurements, suspended organic C, organic N, suspended P, and soluble non-reactive P (SnRP) were calculated for each creek (Figure 5.10).

DOC was the major form of organic carbon species for all nine creeks. It ranged from 91.9% in Bentley Brook to 76.4% in Ten Mile Creek. The distribution of different forms of nitrogen varied among creeks (Figure 5.10B). Willow Brook, Fisher Brook, Dowling Creek, Ten Mile Creek, and Glen Cove had predominantly inorganic N in the form of NO_x; the highest fraction of NO_x is found in Dowling Creek (87.6%). Five Mile Creek, Bentley Brook, Hardscrabble Brook, and Mile Point Creek had almost equal fractions of organic and inorganic ($NO_x + NH_4^+$) nitrogen. The largest fraction of organic N was estimated for Mile Point Creek (61.7%). NH_4^+ was present as a sizable fraction only in Mile Point Creek (3.2%).

Suspended P, on average, was the predominant fraction of P for most creeks, except for Mile Point Creek, Hardscrabble Creek and Ten Mile Creek (Figure 5.10C). The suspended P was between 71.3% (Fisher Brook) and 32.5% (Mile Point Creek). The SRP was the second-highest fraction of all P species. Mile Point Creek had the highest SRP of 59.9%. The SnRP was the least common fraction in the creeks, with Hardscrabble Brook having the highest fraction of SnRP (13.1%); all other creeks have SnRP between 7.7% (Mile Point Creek) and 2.6% (Fisher Brook).

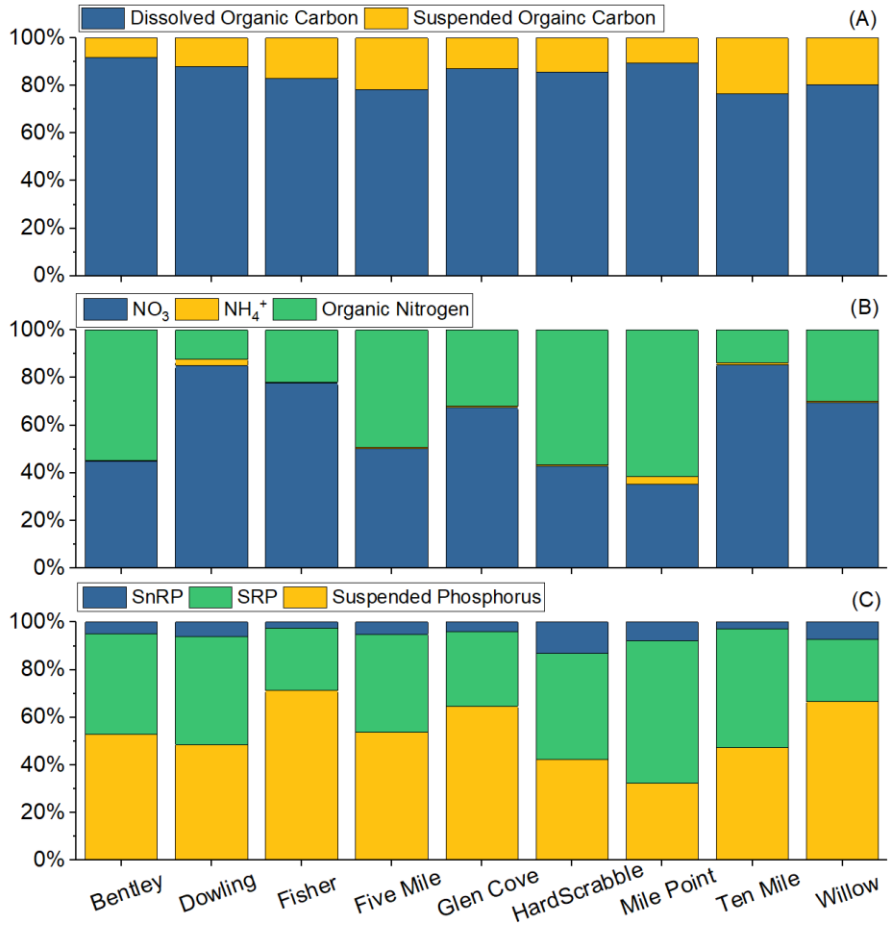

Figure 5.10: The average fractions of the different forms of (A) carbon, (B) nitrogen, and (C) phosphorus in the nine tributaries.

Relationship Between Nutrients

Both N and P are key nutrients in aquatic systems. Their ratio is used to determine the limiting nutrient as well as the potential for excessive phytoplankton growth. Both the mass ratio of TN: TP and the mass ratio of the dissolved forms DIN: SRP were examined.

The TN: TP value in the streams ranged from 14:1 for Mile Point to 51:1 Willow Brook (Figure 5.11A). All creeks were above the freshwater mass threshold value of 11:1. The mass ratio of the bioavailable N and P species ranged from 12:1 for Mile Point Creek to 212:1 and 132:1 for (Figure 5.11B). The Mile Point Creek is the only creek with DIN: SRP ratio close to the

freshwater threshold value of 11:1.

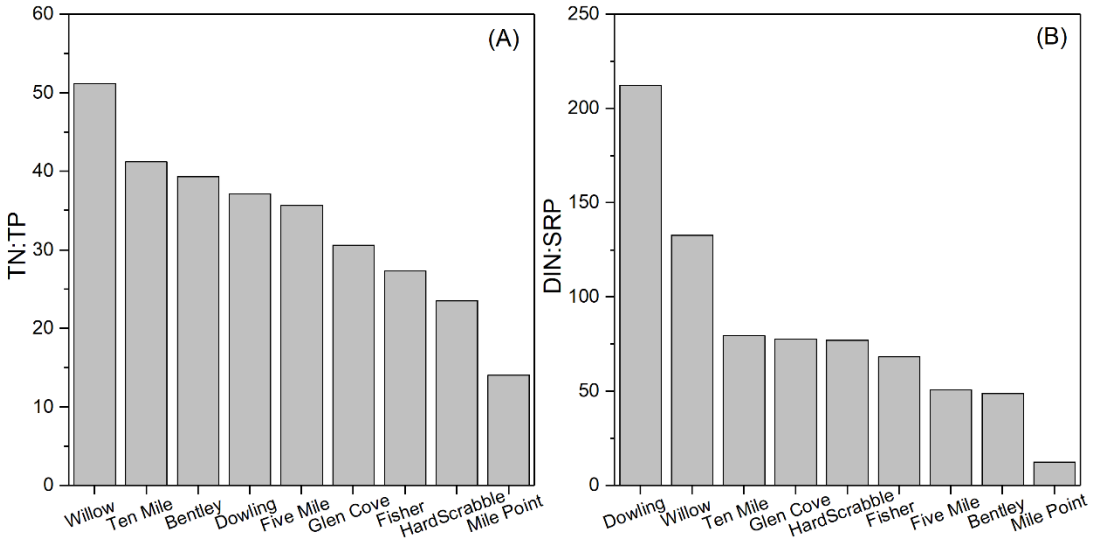

Figure 5.11: (A) Mass ratio of TN: TP and (B) Mass ratio of DIN:SRP of stream chemistry presented in decreasing value.

Discussion

Nutrient concentration in watersheds is controlled by physical settings, land use, weather, and environmental conditions. Healthy amounts of nutrients are essential for the productivity of the ecosystems, but excessive amounts lead to unintended consequences. Here, I infer about the potential hydrological and biogeochemical processes within the watersheds and how they may control the concentration of nutrients in the nine, small, headwater streams of Skaneateles watershed.

Controls of the Organic Carbon Concentration

TOC and DOC appeared to be related to precipitation events. Discharge measurements were not carried out for all the creeks, but precipitation data shows that the highest TOC and DOC

concentrations were observed at precipitation events and the lowest coincided with days without precipitation. The peak in the average seasonal TOC and DOC were observed during the summer of 2019 which had the highest cumulative precipitation. These results corroborate with numerous studies which report that the concentration of organic carbon follow the flow regime (Bass et al., 2011; Guarch-Ribot & Butturini, 2016; Khadka et al., 2014).

Internal (autochthonous) DOC production appears to dominate in all watersheds as the percent DOC from the TOC was 76 - 92%, a range that is at the high end of reported values (65-99%, (Iavorivska, 2016; C. Wang et al., 2021). This hypothesis is also supported by the observed high TOC and DOC concentrations in the creeks during summer-fall compared to lower TOC and DOC concentrations during winter-spring, which suggests microbially-mediated production.

Organic carbon can be delivered to watersheds via direct wet and dry deposition, throughfall input, or litter accumulated on the forest floor. Subsequent decomposition and respiration processes occurring in soils and hyporheic zones produce DOC which is contained in the soil during low flow events but released into the streams during high flow events when lateral flow occurs, and hydrologic paths reconnect. Inamdar et al. (2008) reported that the DOC concentrations in a glaciated, forested stream in Upstate NY, were correlated with groundwater depth. Similarly, Hinton et al. (1997) described the importance of the elevation of the riparian water table in the export of DOC to two small watersheds in Ontario, Canada.

TOC and DOC concentrations were strongly influenced by the physical characteristics of the watershed. Larger and steeper watersheds were associated with lower concentrations of TOC and DOC. Similarly, TOC decreased with the stream order. These patterns suggest that

headwaters have a high influence on the organic carbon concentrations in the studied streams and the increase of the dendritic network and watershed size contribute to decreases in their concentrations (a dilution effect). A deviation from the pattern was observed for two of the creeks, Five Mile Creek and Bentley Brook. Despite that they have the largest watershed area and are third and second order creeks, respectively, they had relatively high TOC and DOC concentrations (Figure 5.3). These two creeks are the only ones with wetlands within their watersheds. Wetlands have been found to be an important source of carbon to streams. Laudon et al. (2004) reported a strong positive correlation between the percent wetland area and the annual average TOC export for six different watersheds. Several other studies reported similar observations (Dillon & Molot, 1997; Hope et al., 1997). Wetlands are rich in biodiversity and bioactivity. They act as a sink for atmospheric carbon and can also enhance the production of DOC (Buytaert et al., 2011). In addition, wetlands are typically slow-moving water systems and offer more time for organic matter to decay, thus increasing carbon output.

Watershed slope alone was able to explain 33% of the variability in TOC and DOC. The observed decrease in the concentration of TOC and DOC with a higher gradient in the terrain most probably was associated with shallower soils. The steeper slope may result in localized and disconnected groundwater flow paths or deeper groundwater circulation (Somers & McKenzie, 2020), shorter flushing times (Creed and Beall 2008), and decreased soil moisture (Ontl and Schulte 2015). After analyzing data from 100 lakes in the Upper Great Lake region, Xenopoulos et al. (2003) found a negative correlation between DOC concentration and watershed slope. Similarly, a study of 70 watersheds in the panarctic region showed a strong negative non-linear dependence of DOC of the watershed slope (Connolly et al., 2018). Gentle

slopes are usually associated with shallower groundwater table (Somers & McKenzie, 2020) and longer residence time (Huntington et al., 2019), which is important for the fate of the organic carbon since wet and inundated areas with longer residence time would stimulate microbial activity, enhance carbon cycling, and facilitate the export of the organic carbon during periods of high flow.

Given all the above, physical and hydrological conditions in the Bentley Brook watershed-having the largest area, lowest slope, high percent wetlands, and being a second order stream-can explain its highest concentrations of organic carbon among all the creeks.

Controls of The Distribution of Nitrogen and Phosphorus Species

The collective evaluation of the concentrations of N and P species defined patterns in their distribution, reflecting the transformations they undergo in the environment. All forms of P appeared to be controlled by the hydrologic regime as the highest concentrations were associated with precipitation events. Nitrogen species had a variable response to precipitation. TN concentrations were higher during precipitation events, while NO_3^- concentrations varied and were lower on most occasions but higher at high intensity or prolonged precipitation. No apparent pattern was evident with NH_4^+. The literature also conveys mixed results. Many studies reported that the dissolved and particulate N and P increase with the increase in streamflow (Inamdar et al. 2008, Dolph et al. 2019, Frei et al. 2020). Only a few studies have reported decreases in NO_3^- concentrations during storm events (Frazar et al. 2019) or lack of a specific pattern between NO_3^- concentrations and flow (Lisboa et al. 2020).

Nitrogen species are not transported conservatively downstream. The change in behavior of NO_3^- in the nine streams appears to be linked to the biogeochemical transformations of N species and the hydrologic regimes. NO_3^- is microbially produced under aerobic conditions via nitrification and can be accumulated in the upper soil layers (Pepper et al. 2011). Under baseflow conditions, groundwater table tends to be low and only deeper groundwater would contribute to nitrogen exchange. The precipitation events with higher intensity and longer duration could elevate the groundwater table, mobilize stored NO_3^-, and transported it to the streams.

The dynamics of phosphorus species appeared to be influenced by geochemical changes and plant growth. The highest concentrations of all P species were measured during precipitation events. Phosphorus has low solubility and is usually associated with the suspended matter (Wetzel 2001). Therefore, concentrations of P in rivers are usually low and high flow events are the primary driver of P export. The dissolution and precipitation of SRP are controlled by Fe oxyhydroxide minerals in soils (Herndon et al. 2020). SRP is bound to Fe minerals under aerobic conditions and is mobilized under anoxic conditions, which are prevalent in saturated soils, hence the observed increase during precipitation events. The SRP in the studied creeks varied between ~30 and 60% of total P. In contrast to nitrogen, concentration of P species varied with the growing season. Enhanced plant uptake during growing season most probably contributed to the decreased P concentration during summer and fall.

An examination of the bi-variant plots between N and P species provided further insight onto the behavior of these nutrients. The relationship between the TN and TP indicated a consistent

pattern. All values were clustered along the N:P= 20:1 line, regardless of the hydrological conditions (Figure 5.12A). Only Fisher brook deviated from this pattern. The TN concentrations in Fisher Creek were unchanging but TP increased during precipitation. The bi-variant plot between the dissolved forms, DIN and SRP exhibited a different pattern - two separate relationships emerged (Figure 5.12B). The datapoints from Bentley Brook, Hardscrabble Creek, Willow Brook, and Dowling Creek consistently fell along the 140:1 line. The distribution of nutrients in these streams cannot be explained by the land use within the watershed because they all are considered primarily agricultural (agricultural land comprises 55-75% of the total area). However, these streams seem to have watersheds with more low land areas because they have the lowest average basin slope (< 5.5%, Figure 5.2). The rest of the creeks had a mixed behavior. Under dry conditions, most of them were clustered along the 20:1 line and shifted to the 140:1 line during precipitation events, associated with higher NO_x and lower SRP. It should be noted that this pattern was not consistent across all watersheds. For instance, during precipitation events, the concentrations of DIN and SRP in Five Mile Creek have been either along the 20:1 line or the 140:1 line. Changes or reconnection of flow paths during precipitation events could have resulted in different behavior of N species in Five Mile Creek.

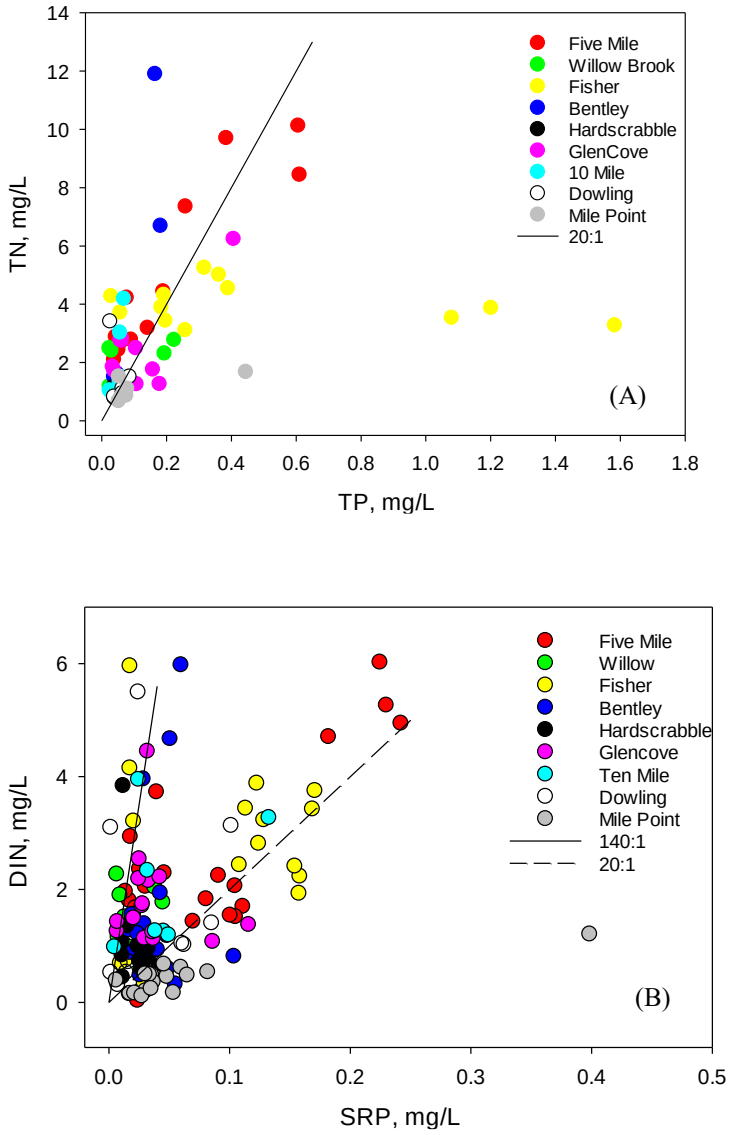

Figure 5.12: Relationships between (A) TN and TP and (B) DIN and SRP in streams or Skaneateles watershed.

Nitrogen and phosphorus are essential elements for aquatic plants and animals, but excess N and P may accelerate eutrophication in streams and lead to undesired algal growth and oxygen deficit. As a measure to control eutrophication, US EPA has established a threshold of 0.05 mg/L for SRP in rivers flowing into lakes (Litke, 1999). A 28% of the SRP concentrations in the studied creeks were above the threshold. The creek with the highest number of SRP exceedances was Fisher Brook (63% of the samples).

In addition to evaluating absolute concentrations, the Redfield ratio, based on the mean elemental composition of marine phytoplankton and stoichiometrically expressed as N:P = 16:1 (7.2:1 on a mass basis), has been widely used as a benchmark to determine limiting nutrient for plant growth. Maranger et al., (2018) proposed that a molar ratio of 25:1 (mass ratios of 11:1) should be used for freshwater ecosystems. In the current study, all creeks have exceeded the mass DIN:SRP ratio for phosphorus limiting growth in freshwater systems. Only Mile Point, the creek with the largest percent developed area, had ratio very close to 11:1. Geider & La Roche (2002) studied both freshwater and marine algae and concluded that in algae, the critical ratio that marks the transition between N- and P-limitation is between 20:1 and 50:1. Except for Mile Point Creek, all studied creeks would be considered P-limited, meaning that algae would assimilate and accumulate P in proportion to the concentration of SRP in water. A recent study that incorporated data from more than 2,000 sampling sites across the U.S. has found that streams draining watersheds with major agricultural and urban developments have a much greater DIN:SRP ratio (Manning et al. 2020). The high DIN:SRP ratio is consistent with the dominant agricultural land use for the nine watersheds (Figure 2.2).

While complex, stream N and P concentrations appear to be controlled by event-scale responses of the streams. Future high-frequency monitoring of the creeks has been planned to assess the response of the streams and implications for management of N and P.

CHAPTER 6 Summary

This thesis was motivated by the recurring problem of HABs plaguing Skaneateles Lake and surrounding watersheds. The issue had been drawing more and more public attention in recent years because of its damaging effects on aesthetics, drinking water safety, tourism, etc. There were two phases to this research. A custom-built multi-parameter unit was designed, built, and deployed to collect physical and hydrological data of Five Mile Creek, a 3rd order tributary of Skaneateles Lake. The retrieved data presented basic physic-chemical characteristics of stream water, including temperature, pH, and DO. The discharge of the stream was calculated combining high-frequency measurements for water level and a rating curve. A pair of HOBO pressure transducers were used to check the functionality of the assembled sensors, and the results showed that the ultrasonic sensor accurately measured water depth. Temperature sensor also worked properly. The pH sensor performed well during low-flow periods, but poorly during high-flow events. As a justification of the reliability of the custom-built multi-parameter unit, I tracked precipitation events and found that major storm events were all recorded. This study demonstrated that a low cost and relatively accurate aquatic monitoring system, could be easily replicated in mass and simply deployed.

The other part of data came from chemical analysis of grab samples. In this analysis, patterns of nutrients concentrations were evaluated among creeks, including their variation with time and season. Nutrients concentration generally followed a seasonal pattern. Carbon and nitrogen species were found at highest concentration in summer and fall, and the highest concentrations of all phosphorus species were found in winter and spring. The mass ratio of DIN and SRP was

above the generally accepted threshold value 11:1, which suggested that P would likely control the growth of algae.

Physical characteristics of the watersheds influenced nutrients distribution in the creeks. Streams with lower stream order had higher concentration of nutrients; the carbon species appeared to be strongly and negatively correlated with watershed area and basin slope. No apparent correlation was observed between N and P species with the physical characteristics of the watersheds, except that streams with low basin slope had higher average DIN:SRP ratio.

It appears that concentration of nutrients in the streams respond to hydrological events and an integrated hydrological and chemical data collection and analyses is needed to predict HAB events. However, in the current study, lack of corresponding data made it impossible to build any meaningful relationship between physical and chemical parameters and estimate loads. In future works, hydrological data should be collected at the same time with samples used for chemical analysis.

This study brought more understanding of the variation of C, N, and P species in creeks draining into Skaneateles Lake and their potential contribution to the exacerbated growth of algae in the lake. The study can help decision-makers identify critical creeks that supply elevated concentration and might be candidates for watershed remediation.

References:

Abbott, R. (2019). 2018 Annual Report Department of Water: Vol. XLIV (Issue April).

Alonso-Andicoberry, C., García-Villada, L., Lopez-Rodas, V., & Costas, E. (2002). Catastrophic mortality of flamingos in a Spanish national park caused by cyanobacteria. *Veterinary Record*, *151*(23), 706–707. https://doi.org/10.1136/vr.151.23.706

Anderson, D. M., Burkholder, J. M., Cochlan, W. P., Glibert, P. M., Gobler, C. J., Heil, C. A., Kudela, R. M., Parsons, M. L., Rensel, J. E. J., Townsend, D. W., Trainer, V. L., & Vargo, G. A. (2008). Harmful algal blooms and eutrophication: Examining linkages from selected coastal regions of the United States. *Harmful Algae*, *8*(1), 39–53. https://doi.org/10.1016/j.hal.2008.08.017

Assendelft, R. S., & Ilja van Meerveld, H. J. (2019). A low-cost, multi-sensor system to monitor temporary stream dynamics in mountainous headwater catchments. *Sensors (Switzerland)*, *19*(21). https://doi.org/10.3390/s19214645

Azevedo, L. B., van Zelm, R., Elshout, P. M. F., Hendriks, A. J., Leuven, R. S. E. W., Struijs, J., de Zwart, D., & Huijbregts, M. A. J. (2013). Species richness-phosphorus relationships for lakes and streams worldwide. *Global Ecology and Biogeography*, *22*(12), 1304–1314. https://doi.org/10.1111/geb.12080

Bass, A. M., Bird, M. I., Liddell, M. J., & Nelson, P. N. (2011). Fluvial dynamics of dissolved and particulate organic carbon during periodic discharge events in a steep tropical rainforest catchment. *Limnology and Oceanography*, *56*(6), 2282–2292. https://doi.org/10.4319/lo.2011.56.6.2282

Beaulieu, J. J., DelSontro, T., & Downing, J. A. (2019). Eutrophication will increase methane emissions from lakes and impoundments during the 21st century. *Nature Communications*, *10*(1), 3–7. https://doi.org/10.1038/s41467-019-09100-5

Behmel, S., Damour, M., Ludwig, R., & Rodriguez, M. J. (2016). Water quality monitoring strategies — A review and future perspectives. *Science of the Total Environment*, *571*, 1312–1329. https://doi.org/10.1016/j.scitotenv.2016.06.235

Bhardwaj, J., Gupta, K. K., & Gupta, R. (2015). A review of emerging trends on water quality

measurement sensors. *Proceedings - International Conference on Technologies for Sustainable Development, ICTSD 2015*. https://doi.org/10.1109/ICTSD.2015.7095919

Brezonik, P., & Arnold, W. (2011). *Water chemistry: an introduction to the chemistry of natural and engineered aquatic systems*. OUP USA.

Buytaert, W., Cuesta-Camacho, F., & Tobón, C. (2011). Potential impacts of climate change on the environmental services of humid tropical alpine regions. *Global Ecology and Biogeography*, *20*(1), 19–33. https://doi.org/10.1111/j.1466-8238.2010.00585.x

Carmichael, W. W., Azevedo, S. M. F. O., An, J. S., Molica, R. J. R., Jochimsen, E. M., Lau, S., Rinehart, K. L., Shaw, G. R., & Eaglesham, G. K. (2001). Human fatalities form cyanobacteria: Chemical and biological evidence for cyanotoxins. *Environmental Health Perspectives*, *109*(7), 663–668. https://doi.org/10.1289/ehp.01109663

Chapman, D. V. (Ed.). (1996). *Water quality assessments: a guide to the use of biota, sediments and water in environmental monitoring.* CRC Press.

Cheung, M. Y., Liang, S., & Lee, J. (2013). Toxin-producing cyanobacteria in freshwater: A review of the problems, impact on drinking water safety, and efforts for protecting public health. *Journal of Microbiology*, *51*(1), 1–10. https://doi.org/10.1007/s12275-013-2549-3

Connolly, C. T., Khosh, M. S., Burkart, G. A., Douglas, T. A., Holmes, R. M., Jacobson, A. D., Tank, S. E., & McClelland, J. W. (2018). Watershed slope as a predictor of fluvial dissolved organic matter and nitrate concentrations across geographical space and catchment size in the Arctic. *Environmental Research Letters*, *13*(10). https://doi.org/10.1088/1748-9326/aae35d

D'Ausilio, A. (2012). Arduino: A low-cost multipurpose lab equipment. *Behavior Research Methods*, *44*(2), 305–313. https://doi.org/10.3758/s13428-011-0163-z

de Montety, V., Martin, J. B., Cohen, M. J., Foster, C., & Kurz, M. J. (2011). Influence of diel biogeochemical cycles on carbonate equilibrium in a karst river. *Chemical Geology*, *283*(1–2), 31–43. https://doi.org/10.1016/j.chemgeo.2010.12.025

Dillon, P. J., & Molot, L. A. (1997). Dissolved organic and inorganic carbon mass balances in central Ontario lakes. *Biogeochemistry*, *36*(1), 29–42. https://doi.org/10.1023/A:1005731828660

Dodds, W. K., Bouska, W. W., Eitzmann, J. L., Pilger, T. J., Pitts, K. L., Riley, A. J., Schloesser, J. T., & Thornbrugh, D. J. (2009). Eutrophication of U. S. freshwaters: Analysis of potential economic damages. *Environmental Science and Technology*, *43*(1), 12–19. https://doi.org/10.1021/es801217q

Dodds, W. K., & Smith, V. H. (2016). Nitrogen, phosphorus, and eutrophication in streams. *Inland Waters*, *6*(2), 155–164. https://doi.org/10.5268/IW-6.2.909

Edmondson, W. T. (1991). Sedimentary record of changes in the condition of Lake Washington. *Limnology and Oceanography, 36*(5), 1031-1043.

EPA. (2013a). Aquatic life ambient water quality criteria for ammonia—Freshwater. (EPA 822-R-18-002). Washington, D.C.: United States Office of Water. Retrieved from https://www.epa.gov/sites/production/files/2015-08/documents/aquatic-life-ambient-water-quality-criteria-forammonia-freshwater-2013.pdf.

Fewtrell, L. (2004). Drinking-water nitrate, methemoglobinemia, and global burden of disease: A discussion. *Environmental Health Perspectives*, *112*(14), 1371–1374. https://doi.org/10.1289/ehp.7216

Frazar, S., Gold, A. J., Addy, K., Moatar, F., Birgand, F., Schroth, A. W., ... & Pradhanang, S. M. (2019). Contrasting behavior of nitrate and phosphate flux from high flow events on small agricultural and urban watersheds. *Biogeochemistry, 145*(1), 141-160.

Frei, R., Abbott, B., Dupas, R., Gu, S., Gruau, G., Thomas, Z., Kolbe, T., Aquilina, L., Labasque, T., Laverman, A., Fovet, O., Moatar, F. and Pinay, G., 2020. Predicting Nutrient Incontinence in the Anthropocene at Watershed Scales. *Frontiers in Environmental Science, 7*.

Geider, R. J., & La Roche, J. (2002). Redfield revisited: Variability of C:N:P in marine microalgae and its biochemical basis. *European Journal of Phycology*, *37*(1), 1–17. https://doi.org/10.1017/S0967026201003456

Glibert, P. M., & Burford, M. A. (2017). Globally changing nutrient loads and harmful algal blooms: recent advances, new paradigms, and continuing challenges. *Oceanography, 30*(1), 58-69.

Grattan, L. M., Holobaugh, S., & Morris, J. G. (2016). Harmful algal blooms and public health.

Harmful Algae, *57*, 2–8. https://doi.org/10.1016/j.hal.2016.05.003

Guarch-Ribot, A., & Butturini, A. (2016). Hydrological conditions regulate dissolved organic matter quality in an intermittent headwater stream. From drought to storm analysis. *Science of the Total Environment*, *571*, 1358–1369. https://doi.org/10.1016/j.scitotenv.2016.07.060

Hall, J., Zaffiro, A. D., Marx, R. B., Kefauver, P. C., Krishnan, E. R., Haught, R. C., & Herrmann, J. G. (2007). On–Line water quality parameters as indicators of distribution system contamination. *Journal-American Water Works Association, 99*(1), 66-77.

Hayashi, M., Vogt, T., Mächler, L., & Schirmer, M. (2012). Diurnal fluctuations of electrical conductivity in a pre-alpine river: Effects of photosynthesis and groundwater exchange. *Journal of Hydrology, 450*, 93-104.

Herndon, E., Kinsman-Costello, L., Di Domenico, N., Duroe, K., Barczok, M., Smith, C., & Wullschleger, S. D. (2020). Iron and iron-bound phosphate accumulate in surface soils of ice-wedge polygons in arctic tundra. *Environmental Science: Processes & Impacts, 22*(7), 1475-1490.

Hinton, M. J., Schiff, S. L., & English, M. C. (1997). The Significance of Storms for the Concentration and Export of Dissolved Organic Carbon from Two Precambrian Shield Catchments Author (s): M . J . Hinton , S . L . Schiff and M . C . English Source : Biogeochemistry , Vol . 36 , No . 1 , Dissolved Organ. *Biogeochemistry*, *36*(1), 67–88.

Ho, J. C., & Michalak, A. M. (2015). Challenges in tracking harmful algal blooms: A synthesis of evidence from Lake Erie. *Journal of Great Lakes Research*, *41*(2), 317–325. https://doi.org/10.1016/j.jglr.2015.01.001

Ho, J. C., Michalak, A. M., & Pahlevan, N. (2019). Widespread global increase in intense lake phytoplankton blooms since the 1980s. *Nature*, *574*(7780), 667–670. https://doi.org/10.1038/s41586-019-1648-7

Hope, D., Billett, M. F., & Cresser, M. S. (1997). Exports of organic carbon in two river systems in NE Scotland. *Journal of Hydrology*, *193*(1–4), 61–82. https://doi.org/10.1016/S0022-1694(96)03150-2

Huntington, T. G., Roesler, C. S., & Aiken, G. R. (2019). Evidence for conservative transport of dissolved organic carbon in major river basins in the Gulf of Maine Watershed. *Journal of Hydrology*, *573*, 755–767. https://doi.org/10.1016/j.jhydrol.2019.03.076

Iavorivska, L. (2016). *Dissolved Organic Matter in Atmospheric Deposition: Inputs to Watersheds and Influences of Climate.* The Pennsylvania State University.

Inamdar, S., Rupp, J., & Mitchell, M. (2008). Differences in dissolved organic carbon and nitrogen responses to storm-event and ground-water conditions in a forested, glaciated watershed in western New York. *Journal of the American Water Resources Association*, *44*(6), 1458–1473. https://doi.org/10.1111/j.1752-1688.2008.00251.x

Khadka, M. B., Martin, J. B., & Jin, J. (2014). Transport of dissolved carbon and CO2 degassing from a river system in a mixed silicate and carbonate catchment. *Journal of Hydrology*, *513*, 391–402. https://doi.org/10.1016/j.jhydrol.2014.03.070

Koreiviene, J., Anne, O., Kasperovičiene, J., & Burškyte, V. (2014). Cyanotoxin management and human health risk mitigation in recreational waters. In *Environmental Monitoring and Assessment* (Vol. 186, Issue 7, pp. 4443–4459). https://doi.org/10.1007/s10661-014-3710-0

Laudon, H., Köhler, S., & Buffam, I. (2004). Seasonal TOC export from seven boreal catchments in northern Sweden. *Aquatic Sciences*, *66*(2), 223–230. https://doi.org/10.1007/s00027-004-0700-2

Lisboa, M. S., Schneider, R. L., Sullivan, P. J., & Walter, M. T. (2020). Drought and post-drought rain effect on stream phosphorus and other nutrient losses in the Northeastern USA. *Journal of Hydrology: Regional Studies, 28*, 100672.

Litke, D. W. (1999). Review of phosphorus control measures in the United States and their effects on water quality: US Geological Survey Water-Resources Investigations Report 99-4007. *South Carolina: US Geological Survey Fact Sheet FS-007–98.*

Manning, D. W., Rosemond, A. D., Benstead, J. P., Bumpers, P. M., & Kominoski, J. S. (2020). Transport of N and P in US streams and rivers differs with land use and between dissolved and particulate forms. *Ecological Applications, 30*(6), e02130.

Maranger, R., Jones, S. E., & Cotner, J. B. (2018). Stoichiometry of carbon, nitrogen, and

phosphorus through the freshwater pipe. *Limnology and Oceanography Letters*, *3*(3), 89–101. https://doi.org/10.1002/lol2.10080

Michel, R. L., & Kraemer, T. F. (1995). Use of isotopic data to estimate water residence times of the Finger Lakes, New York. *Journal of Hydrology*, *164*(1–4), 1–18. https://doi.org/10.1016/0022-1694(94)02586-Z

Moss, B., Jeppesen, E., Søndergaard, M., Lauridsen, T. L., & Liu, Z. (2013). Nitrogen, macrophytes, shallow lakes and nutrient limitation: Resolution of a current controversy? *Hydrobiologia*, *710*(1), 3–21. https://doi.org/10.1007/s10750-012-1033-0

Mulyana, Y., & Hakim, D. L. (2018). Prototype of Water Turbidity Monitoring System. *IOP Conference Series: Materials Science and Engineering*, *384*(1). https://doi.org/10.1088/1757-899X/384/1/012052

Neary, D. G., Ice, G. G., & Jackson, C. R. (2009). Linkages between forest soils and water quality and quantity. *Forest Ecology and Management*, *258*(10), 2269–2281. https://doi.org/10.1016/j.foreco.2009.05.027

Niekerk, H. Van. (2004). UNEP Global Environmental Monitoring System/Water Programme :South African Monitoring Programme Design. November.

NYSDEC. (2017). 2017 FINGER LAKES Summary of Historic Finger Lakes Data and the 2017 (Issue September 2018).

Osman, S. O., Mohamed, M. Z., Suliman, A. M., & Mohammed, A. A. (2018). Design and Implementation of a Low-Cost Real-Time In-Situ Drinking Water Quality Monitoring System Using Arduino. *2018 International Conference on Computer, Control, Electrical, and Electronics Engineering, ICCCEEE 2018*, 0–6. https://doi.org/10.1109/ICCCEEE.2018.8515886

Otten, T. G., & Paerl, H. W. (2011). Phylogenetic Inference of Colony Isolates Comprising Seasonal Microcystis Blooms in Lake Taihu, China. *Microbial Ecology*, *62*(4), 907–918. https://doi.org/10.1007/s00248-011-9884-x

Paerl, H. W., & Otten, T. G. (2013). Harmful Cyanobacterial Blooms: Causes, Consequences, and Controls. *Microbial Ecology*, *65*(4), 995–1010. https://doi.org/10.1007/s00248-012-0159-y

Paerl, H. W., Otten, T. G., & Kudela, R. (2018). Mitigating the Expansion of Harmful Algal Blooms Across the Freshwater-to-Marine Continuum. *Environmental Science and Technology*, *52*(10), 5519–5529. https://doi.org/10.1021/acs.est.7b05950

Pepper, I. L., Gerba, C. P., Gentry, T. J., & Maier, R. M. (Eds.). (2011). *Environmental microbiology*. Academic press.

Potter, B. B., & Wimsatt, J. (2009). Method 415.3, Rev. 1.2: Determination of Total Organic Carbon and Specific UV Absorbance at 254 nm in Source Water and Drinking Water. *US EPA, Washington*.

Poulsen, R., Cedergreen, N., Hayes, T., & Hansen, M. (2018). Nitrate: An environmental endocrine disruptor? A review of evidence and research needs. *Environmental Science & Technology, 52*(7), 3869–3887. https://doi.org/10.1021/acs.est.7b06419

Pu, J., Li, J., Khadka, M. B., Martin, J. B., Zhang, T., Yu, S., & Yuan, D. (2017). In-stream metabolism and atmospheric carbon sequestration in a groundwater-fed karst stream. *Science of the Total Environment*, *579*(50), 1343–1355. https://doi.org/10.1016/j.scitotenv.2016.11.132

Rabalais, N. N. (2002). Nitrogen in aquatic ecosystems. *Ambio*, *31*(2), 102–112. https://doi.org/10.1579/0044-7447-31.2.102

Redfield, A. C. (1958). Redfield_AmSci_1958.pdf. In *American Scientist*.

Rodriguez-Mozaz, S., Lopez De Alda, M. J., & Barceló, D. (2006). Biosensors as useful tools for environmental analysis and monitoring. *Analytical and Bioanalytical Chemistry*, *386*(4), 1025–1041. https://doi.org/10.1007/s00216-006-0574-3

Sawaya, K. (2003). Extending satellite remote sensing to local scales: land and water resource monitoring using high-resolution imagery. *Remote Sensing of Environment*, *88*, 144–156. https://doi.org/10.1016/j.rse.2003.04.0006

Schindler, D. W., Hecky, R. E., Findlay, D. L., Stainton, M. P., Parker, B. R., Paterson, M. J., Beaty, K. G., Lyng, M., & Kasian, S. E. M. (2008). Eutrophication of lakes cannot be controlled by reducing nitrogen input: Results of a 37-year whole-ecosystem experiment. *Proceedings of the National Academy of Sciences of the United States of America*, *105*(32), 11254–11258. https://doi.org/10.1073/pnas.0805108105

Somers, L. D., & McKenzie, J. M. (2020). A review of groundwater in high mountain environments. *Wiley Interdisciplinary Reviews: Water*, *7*(6), 1–27. https://doi.org/10.1002/wat2.1475

Stewart, I., Seawright, A. A., & Shaw, G. R. (2008). Cyanobacterial poisoning in livestock, wild mammals and birds--an overview. *Advances in Experimental Medicine and Biology*, *619*, 613–637. https://doi.org/10.1007/978-0-387-75865-7_28

Strobl, R. O., & Robillard, P. D. (2008). Network design for water quality monitoring of surface freshwaters: A review. *Journal of Environmental Management*, *87*(4), 639–648. https://doi.org/10.1016/j.jenvman.2007.03.001

Tank, J. L., & Dodds, W. K. (2003). Nutrient limitation of epilithic and epixylic biofilms in ten North American streams. *Freshwater Biology*, *48*(6), 1031–1049. https://doi.org/10.1046/j.1365-2427.2003.01067.x

Trevathan, J., Read, W., & Schmidtke, S. (2020). Towards the development of an affordable and practical light attenuation turbidity sensor for remote near real-time aquatic monitoring. *Sensors (Switzerland)*, *20*(7). https://doi.org/10.3390/s20071993

Van Nieuwenhuyse, E. E., & Jones, J. R. (1996). Phosphorus chlorophyll relationship in temperate streams and its variation with stream catchment area. *Canadian Journal of Fisheries and Aquatic Sciences, 53*(1), 99-105.

Vander Zanden, M. J., & Vadeboncoeur, Y. (2002). Fishes as Integrators of Benthic and Pelagic Food Webs in Lakes Author (s): M . Jake Vander Zanden and Yvonne Vadeboncoeur Published by : Wiley Stable URL : http://www.jstor.org/stable/3072047 REFERENCES Linked references are available on JSTOR for this. *Ecology*, *83*(8), 2152–2161.

Wang, C., Zhong, W., Ping, W., Lin, Z., Wang, R., Dai, J., Guo, M., Xiong, W., Zhao, J. C., & Hu, L. (2021). Rapid Synthesis and Sintering of Metals from Powders. *Advanced Science*, *2004229*, 1–6. https://doi.org/10.1002/advs.202004229

Wang, Y., Rajib, S. M. S. M., Collins, C., & Grieve, B. (2018). Low-Cost Turbidity Sensor for Low-Power Wireless Monitoring of Fresh-Water Courses. *IEEE Sensors Journal*, *18*(11), 4689–4696. https://doi.org/10.1109/JSEN.2018.2826778

Wetzel, R. G. (2001). *Limnology: lake and river ecosystems.* gulf professional publishing.

World Health Organization. (2003). *Guidelines for safe recreational water environments: Coastal and fresh waters* (Vol. 1). World Health Organization.

Wu, Z., Wang, J., Bian, C., Tong, J., & Xia, S. (2020). A MEMS-based multi-parameter integrated chip and its portable system forwater quality detection. *Micromachines*, *11*(1). https://doi.org/10.3390/mi11010063

Xenopoulos, M. A., Lodge, D. M., Frentress, J., Kreps, T. A., Bridgham, S. D., Grossman, E., & Jackson, C. J. (2003). Regional comparisons of watershed determinants of dissolved organic carbon in temperate lakes from the Upper Great Lakes region and selected regions globally. *Limnology and Oceanography*, *48*(6), 2321–2334. https://doi.org/10.4319/lo.2003.48.6.2321

Zhang, F., Lee, J., Liang, S., & Shum, C. (2015). Cyanobacteria blooms and non-alcoholic liver disease: Evidence from a county level ecological study in the United States. *Environmental Health: A Global Access Science Source*, *14*(1), 1–11. https://doi.org/10.1186/s12940-015-0026-7

Vita

EDUCATION

MENGYI ZHANG (MZHANG62@SYR.EDU)

Syracuse University, Syracuse, NY

M.S. in *Environmental Engineering*, College of Engineering and Computer Science — Anticipated: May 2019

- Graduate student grant
- courses: Physical Hydrology, Environmental Organic Chemistry, Geographic Information System, Building Environmental Modeling, Water Treatment Process, Air Resources, Applied Environmental Microbiology, and Physical Cell Biology

Qingdao Technological University, Shandong, China

B.S. in *Engineering* — June 2017

- Major: Architectural Environment & Energy Application Engineering
- Relevant courses: Advanced Mathematics, Physics, Engineering Mechanics, Engineering Thermodynamics, Heat Transfer, Fluid dynamics

SKILLS

- Design Software: ArcGIS, AutoCAD, BIM system
- Technical and Laboratory Machines: Organic Carbon Analyzer Apollo 9000, AA (Atomic Absorption Analysis) Winlab Analyst 300, Sampling
- Languages: English and Mandarin

ACADEMIC PROJECTS

Sensor for Early-Warning System for Harmful Algal Blooms — Nov. 2018 – Present

Syracuse University, Department of Environmental Engineering

- Built sensor boxes with teammates from Computer Science Department, measure water quality index including pH, DO, and temperature base on Arduino
- Ran the prototype in lab, and documented experimental data and results which will be followed some work on field in Skaneateles
- Field work in Skaneateles tributaries every week, doing gaging and sample collecting
- Ran samples in Flow Analyzer and Apollo Analyzer to measure water quality including DOC, phosphate and other chemicals

The Evaluation of Human Body Comfortable Degree under Low Pressure Environment — Sep. 2014 – Jan. 2015

Qingdao Technological University, Department of Environment

- Designed and collected questionnaires about feelings of indoor environment in our simulation cabin from volunteers and documented results
- Built thermal sensation model based on environmental parameter and modified the model according to volunteers' feedback

Integration Research on Passive Villa Architecture in Qingdao — Mar. 2016 – Dec. 2016

Qingdao Technological University, Department of Environment

- Guided the team to simulate the energy consumption of architecture under the new energy technology environment
- Built the model of passive architecture with the DeST software to find out the improvement directions and optimal design

PROFESSIONAL EXPERIMENT

Department of Civil and Environmental Engineering, Syracuse University — Jan. 2019 – Present

Teaching Assistant (Grader)

- Graded assignments, Course: Water Resources Engineering, and reported feedback to Professor in one week
- Assisted another TA in Recitation and supported students in analyzing course problems and identifying solutions.

Sinopec Petroleum Engineering Design Company — Jun. 2016 – Aug. 2016

Assistant

- Learned the practical design regulations of heating and air conditioning, and commanded the method of getting useful parameters such as regional meteorological data and heat transfer resistance
- Commanded the basic operations of Hongye System to calculate the thermal load of building and obtained data

AWARDS

EMPOWER, Syracuse University — Sep. 2019

- EMPOWER Trainee

Technology Innovation Scholarship of Qingdao Technological University — Oct. 2017

Qingdao Technological University, Department of Environment

- Founded Environment Protection Group in department to publicize the importance of energy saving, and brought up ideas for environment protection

Excellent Intern of Qingdao City Construction Group, Qingdao Technological University, Department of Environment — Jun. 2016

- Conducted research on building passive villa in Qingdao

Outstanding Volunteer of Qingdao Technological University, Qingdao Technological University, Department of Environment — Feb. 2015